Table 2 Patients' profile in benign cases

Case no.	Age	Gender	Plasma glucose level (mg/dl)	Final diagnosis		PET results
37	70	F	291	Lung cancer, post-operative state	No recurrence	TN
38	66	F	265	Breast cancer, post-operative state	Physiological bowel uptake	FP
39[a]	66	F	205	Pancreas cancer, post-chemotherapy	No recurrence	TN
40	67	F	295	Lung cancer, post-operative state	No recurrence	TN
41	58	M	298	Pancreas cancer, post-operative state	No recurrence	TN
42[a]	58	M	225	Hepatocellular carcinoma, post-operative state	No recurrence	TN
43	41	M	267	Malignant lymphoma, post-chemotherapy	No recurrence	TN
44	70	F	229	Cervical cancer, post-operative state	No recurrence	TN
45	56	M	217	Hepatocellular carcinoma, post-TACE	Biloma	FP
46	68	M	242	Pancreas cancer, post-operative state	No recurrence	TN
47[a]	72	M	666	Pancreas cancer, post-operative state	No recurrence	TN
48	54	M	299	Laryngeal cancer, post-operative state	No recurrence	TN

TACE transcatheter arterial chemotherapeutic embolization

[a] Same patients shown as different cases in Table 1 (No. 39 = No. 36, No. 42 = No. 11, No. 47 = No. 27)

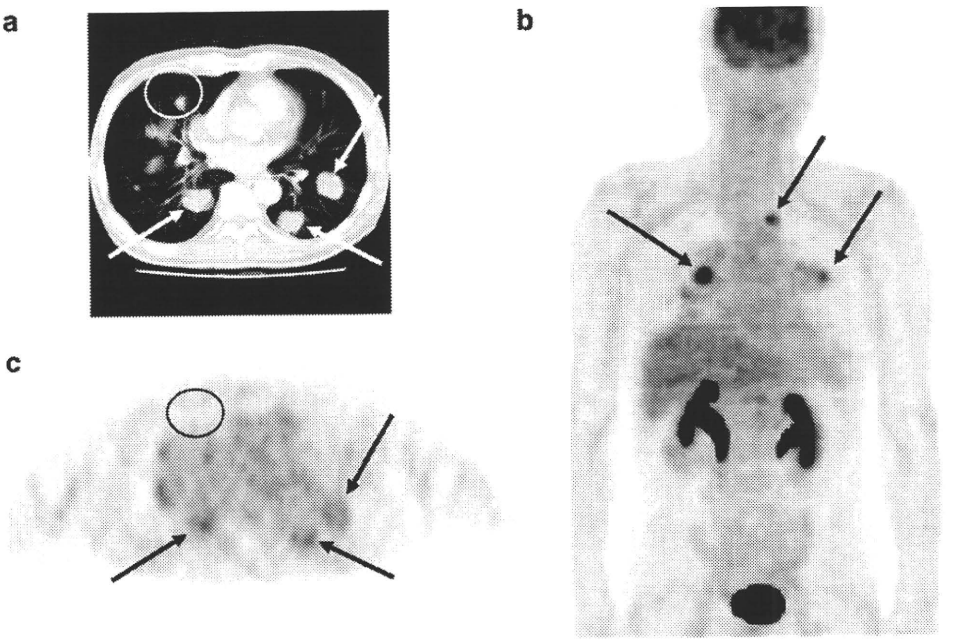

Fig. 1 A 64-year-old diabetic male with multiple lung metastases (patient#7). The plasma glucose level on administration of FDG was 291 mg/dl. CT (**a**) shows multiple pulmonary nodules in bilateral lung fields (**a**), and moderate to intense uptake is seen on PET (**b** MIP image, **c** axial image), demonstrating multiple lung metastases. Most of the nodules (up to 5 lesions) in the lung fields (*white arrows*) were demonstrated on PET in the corresponding area (*black arrows*), while a small nodule in the right middle lobe was not demonstrated on PET (*white* and *black circles*). However, it is unknown whether this small lesion was clearly depicted under normoglycemia or not, because the size of the lesion was too small

1.3 ± 0.3) in the randomly chosen 50 patients with normoglycemia (Fig. 3c, d). These results suggest that FDG uptake in cancer tissue under hyperglycemia can be kept relatively high, despite high plasma glucose level and the decrease in brain FDG uptake.

Discussion

Our results suggested that tumor FDG uptake maintains a sufficiently high level for visual clinical diagnosis in a majority of cases (except for low FDG-avid tumors or

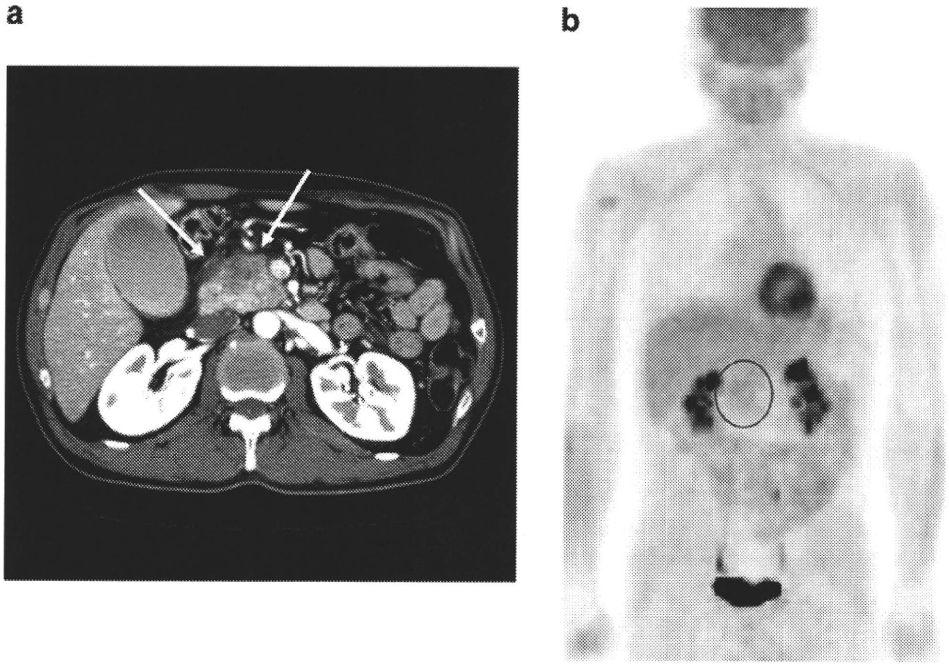

Fig. 2 A 69-year-old diabetic male with pancreatic cancer (patient#30). The plasma glucose level on administration of FDG was 212 mg/dl. CT revealed a mass in the pancreatic head portion (**a** *white arrow*); however, only faint uptake was just observed in the corresponding area with SUVmax of 2.4 (**b** MIP image, *black circle*). Pancreatic cancer of 35 mm in size was confirmed by surgery. Pathological examination revealed that the tumor was tubular adenocarcinoma of the scirrhous type

Table 3 Lesion-based analysis of false-negative lesions

	Case no.	Diagnosis	Primary lesion	Post-treatment	Pathology	SUVmax	Tumor size (mm)
Primary lesion							
1	30	Pancreas cancer	–	–	Scirrhous type	2.4	35
2	11	Hepatocellular carcinoma	–	–	Well-differentiated	2.9	25
3	18	Lung cancer	–	Post-chemotherapy	Adenocarcinoma	2.1	25
4	13	Hepatocellular carcinoma	–	–	Well-differentiated	3.4	22
5	12	Hepatocellular carcinoma	–	–	Poorly differentiated	1.8	14
6	2	Bile duct cancer	–	–	Moderately differentiated	3.8	Small
Additional lesion							
1	21	Bone metastasis	Lung cancer	–	Osteoblastic	2.7	40
2	21	Bone metastasis	Lung cancer	–	Osteoblastic	na	30
3	3	Bone metastasis	Breast cancer	Post-radiotherapy	–	na	30
4	22	GGO (lung), double primary	Lung cancer	–	Well-differentiated	na	17
5	13	Liver metastasis or triple primary	Hepatocellular carcinoma	–	Well-differentiated	2.9	15
6	13	Liver metastasis or triple primary	Hepatocellular carcinoma	–	Well-differentiated	na	13
7	35	Lymph node metastasis	Pancreas cancer	–	Moderately differentiated	na	11
8	32	Liver metastasis	Pancreas cancer	–	Moderately differentiated	3.9	9
9	29	Lymph node metastasis	Pancreas cancer	–	Moderately differentiated	na	7
10	34	Lymph node metastasis	Pancreas cancer	–	Moderately differentiated	2.5	5
11	1	Lung metastasis	Adrenal cancer	–	Unknown	na	3
12	18	Lymph node metastasis	Lung cancer	Post-chemotherapy	Unknown	na	Small
13	33	Liver metastasis	Pancreas cancer	–	Moderately differentiated	na	Small

na not available

Lesion size was not measured in some lesions because imaging findings did not depict the lesions and there was no information on pathological reports

small lesions) with chronic hyperglycemia (more than 200 mg/dl). Thirty of 36 patients showed positive results in the main tumor. Overall, the patient-based diagnosis was with a high level of accuracy, as sensitivity, specificity, positive predictive value, negative predictive value and diagnostic accuracy were 83, 83, 94, 63, and 83%,

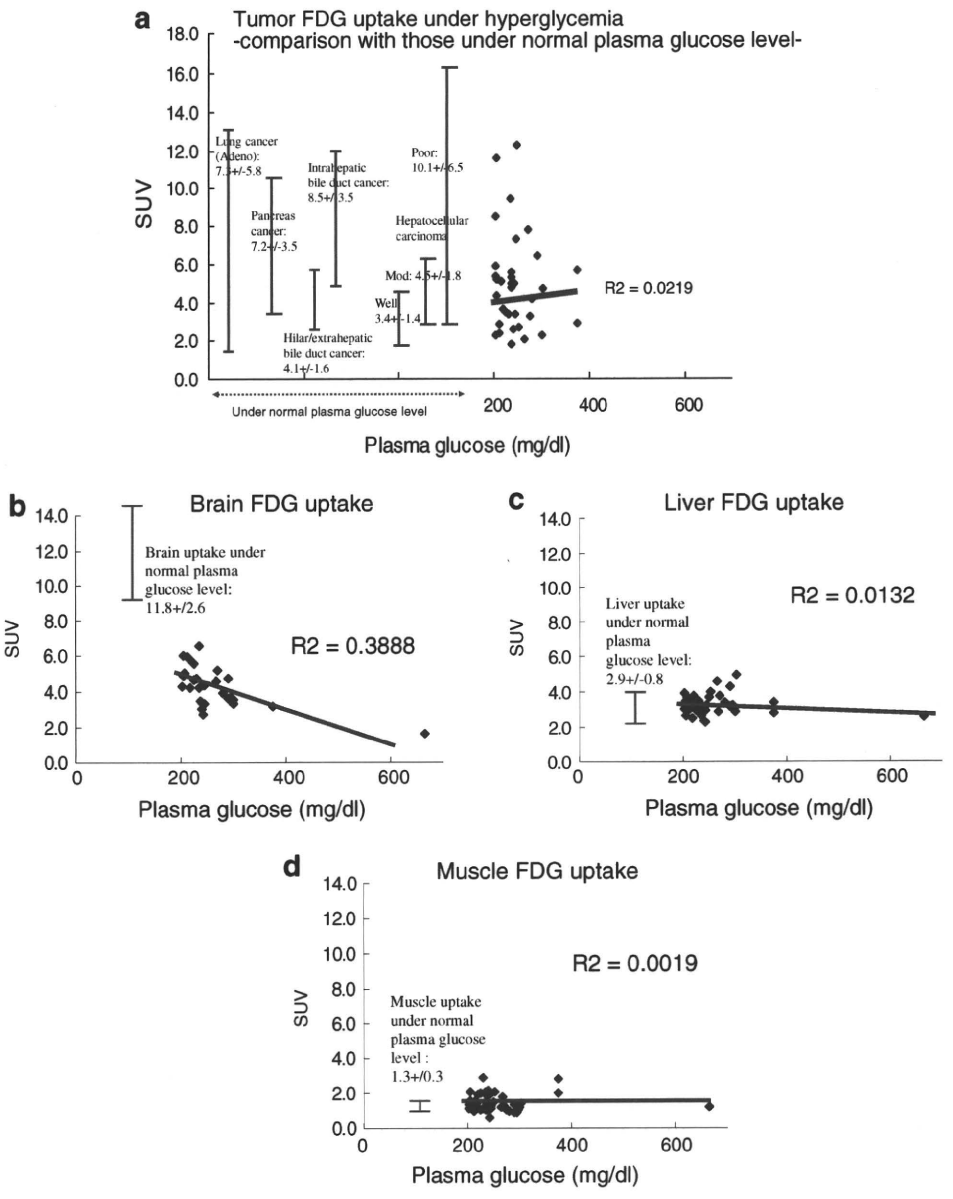

Fig. 3 Scatter gram for SUV and plasma glucose level in tumor and each organ. The relationship between FDG uptake and plasma glucose level was shown in tumor (**a**), brain (**b**), liver (**c**) and muscle (**d**). (**a**) Regarding tumor FDG uptake, SUV ranged widely from 1.8 to 12.8. Even under high plasma glucose level, most of the tumors showed FDG uptake higher than 3.0 and there was no significant correlation between SUV and plasma glucose level (R^2 0.0219). Seven perpendicular bars were also shown on the left side of the scattered dots, which represented the average ± SD of SUV calculated in each cancer under normal plasma glucose level in our institute (see "Discussion"). On the other hand, the brain showed negative relationship with plasma glucose levels. Brain FDG uptake (SUVmax = 4.5 ± 1.0) ranged from 1.6 to 6.6, which was significantly lower than those in the normoglycemic patients (SUV = 11.8 ± 2.6). There was a significant inverse correlation between brain SUV and plasma glucose level (R^2 0.3888). FDG uptake of liver and muscle was quite stable in the hyperglycemic condition. There was no significant correlation between liver and muscle FDG uptake and plasma glucose level (R^2; liver: 0.0132, muscle: 0.0019)

respectively. In both lung cancers and pancreatic cancers, tumor detectability was 91% with only one false-negative case, which was a satisfactory level for clinical oncologic diagnosis even under normoglycemia. Lesion-based diagnosis also showed high sensitivity (74%). This result is compatible with those of previous studies performed with lung cancers and uterine cervix cancers [10, 11]. It means that in a majority of clinical situations, FDG-PET study could be performed despite the high plasma glucose level, if the high glucose level was introduced due to chronic hyperglycemia.

In this investigation, it must be noted that about one-third of FDG-negative lesions (6/19 lesions) consisted of low FDG-avid lesions and that about two-thirds (11/19 lesions) consisted of small lesions (less than 15 mm) (Table 3). Pancreatic cancer sometimes shows relatively low FDG accumulation, mainly because of its desmoplastic pathological character and the resultant low tumor cell cellularity [12]. Well-differentiated hepatocellular carcinoma is known for its relatively low detection rate, because well-differentiated cancers tend to have lower FDG accumulation than those of poorly differentiated cancers [13, 14]. Osteoblastic bone metastases frequently had low FDG uptake [15]. Well-differentiated adenocarcinoma of lung with ground-glass opacity is known to have low FDG avidity [16]. Thus, these low FDG-avid pathological characters may be one of the main causes of false-negative results in this study. Regarding small lesions (smaller than 15 mm in size), it is not the problem of the plasma glucose level, but the problem of the resolution of the PET device.

In these false negative cases, recent advance of PET/CT or PET scan using breath-hold technique, etc., may hammer out a solution, regardless of plasma glucose level.

Let us check the six false-negative primary lesions in detail (Table 3). First of all, a case of pancreatic cancer showed lower FDG uptake. According to the previously published data of our institute, the averages of SUVmax under normoglycemia in pancreatic cancer were 7.2 ± 3.5 [13]. Therefore, the SUV = 2.4 was relatively low for a common invasive ductal adenocarcinoma of the pancreas (Fig. 3a). However, not only hyperglycemia, but also the scirrhous pathological character may affect FDG uptake, because of the low tumor cell cellularity. Secondly, three false-negative cases with hepatocellular carcinomas should be discussed (patient#11–13). According to the previously published data of our institute, the averages of SUVmax under normoglycemia in well, moderate and poorly differentiated hepatocellular carcinoma were 3.4 ± 1.4, 4.5 ± 1.8 and 10.1 ± 6.5, respectively [13]. The average SUV of normal liver was also shown to be 2.9 ± 0.8; therefore, well-differentiated hepatocellular carcinoma shows almost the same FDG uptake as that of the normal liver tissue (Fig. 3a, c). The three cases in this study showed the pathology, SUV and tumor size as follows: patient#11, well, SUV = 2.9 and 25 mm; patient#13, well, SUV = 3.4 and 22 mm; patient#12, poor, SUV = 1.8 and 14 mm, respectively. We suspected that the former two cases were false negative in PET scan due to the well-differentiated pathological character of the tumor. We also suspected that the latter case with poorly differentiated type showed negative PET finding mainly due to the small size. Thirdly, the false-negative result of patient#18 with lung cancer was due to chemotherapeutic effect. The pathology of patient#18 was not obtained, because this patient was treated with systemic chemotherapy, but the cytology by pretreatment bronchoscopy revealed adenocarcinoma, which is known to be a relatively lower FDG-avid tumor. According to the previously published data of our institute, the averages of SUVmax under normoglycemia in adenocarcinoma (AC) and squamous cell carcinoma (SCC) of lung were 7.3 ± 5.8, 15.2 ± 4.7, respectively [17]. The SUV = 2.1 in this case was relatively low for a common adenocarcinoma of the lung (Fig. 3a). However, this patient had received chemotherapy 2 weeks before the PET scan and that was why PET showed false-negative result. Bile duct cancer (patient#2; hilar bile duct cancer) also is discussed. According to previously published and in-house data of our institute, the averages of SUVmax of intrahepatic and hilar/extrahepatic bile duct cancer under normoglycemia were 8.5 ± 3.5 and 4.1 ± 1.6, respectively [17]. The SUV of 3.8 in this case was not as low, compared to the average of hilar/extrahepatic bile duct cancers (Fig. 3a). Hilar and extrahepatic cholangiocarcinomas diagnosed by obstructive jaundice tend to be small in size; therefore, their FDG uptake was usually lower than that of the intrahepatic one. The tumor size of patient#2 was also small and thin, and the accurate size was not available in the pathological report. The result of false-negative PET scan in this case may be due to the small size of the tumor.

In the additional 13 lesions with false-negative result (Table 3), the first 4 lesions with larger tumor size were suspected to have low FDG avidity, due to osteoblastic character (bone metastasis), post-radiation (bone metastasis) and well-differentiated character (GGO). The following two lesions of small size were hepatocellular carcinoma with well-differentiated character (patient#13). The other negative lesions were less than 11 mm in size.

Therefore, we could conclude that FDG accumulation in the FDG-avid tumor of a certain size (larger than 15 mm) remained sufficiently high for visual diagnosis in the majority of cases even under chronic hyperglycemia. On the other hands, FDG diagnosis at the time of chronic hyperglycemia must be performed carefully in cases of low FDG-avid tumors, such as pancreatic cancers, hepatocellular carcinomas and well-differentiated lung adenocarcinomas. In addition, clinicians should pay attention to the possibility of the presence of false-negative small-sized lesions at the time of chronic hyperglycemia.

Diabetes mellitus, especially type 2, is now found in almost every population. A variety of evidence suggests that without effective prevention and control program, the prevalence will continue to increase globally [18]. Patients with diabetes are known to be at risk of several cancers. There is increasing evidence that diabetes and/or hyperglycemia are independent risk factors and/or predictors at least in respect of cancer of the colon, pancreas, female breast and endometrium and, in men, of the liver and bladder [19]. In the present study, we encountered only 1% of chronic hyperglycemic patients in 5 years of clinical experience, but much more cancer patients with hyperglycemia or uncontrolled diabetes may be expected in the near future.

In general, FDG-PET has not been performed in known diabetic patients having cancers, because of the evidences from several papers, which suggest poor diagnostic results due to hyperglycemia. However, most of previous papers did not pay attention to the type of hyperglycemia, acute or chronic. When a nuclear physician encounters a patient with unexpected hyperglycemia in clinical FDG-PET study, he needs to find out the cause of hyperglycemia: acute hyperglycemia caused by insufficient fasting or chronic hyperglycemia under fasting condition caused by diabetes. For patients with insufficient fasting, it is recommended to reschedule and perform the PET scan under appropriate fasting condition at a later date. If patients had hyperglycemia caused by severe or poorly controlled

diabetes, PET scan may not be canceled and can be performed after obtaining permission of the referring physician. Also, the consent of the patient, informing the possibility of false-negative results, has to be obtained. PET scan is performed without delay because (1) re-examination at a later date after treatment for diabetes would cause a possible delay in the treatment, especially in patients with an aggressive cancer, such as pancreatic cancer; (2) even under hyperglycemia, FDG-PET has a satisfactory diagnostic performance and may detect unexpected distant metastasis or may show other useful information.

Contrary to the results of tumors, there was an inverse correlation between brain FDG uptake and blood glucose level (Fig. 3). Although glucose is the only energy source of brain tissue, chronic hyperglycemia is known to have deleterious effects on brain tissue because excessive influx of glucose results in increased intracellular protein glycation and generation of free radicals [20, 21]. A variety of natural protective mechanisms against hyperglycemia have been investigated and many researches using animal model are focusing on glucose transporters' expression on blood–brain barrier (BBB) [22, 23]. In brain tissue, vascular endothelial and vascular smooth muscle cells express the ubiquitous GLUT-1 predominantly, and these cells autoregulate their rate of glucose transport in response to changes in ambient glucose levels. This results in the decrease of transport up to 50%, by reduction of GLUT-1 expression on exposure to high glucose levels [24]. Our results are supposed to be compatible with these animal studies.

In the present study, the muscle and liver uptakes were kept stable in the hyperglycemic condition (>200 mg/dl) (Fig. 3). Chronic hyperglycemia is known to have deleterious effects on muscle cells [25]. Muscle cells may have a natural protective mechanism against hyperglycemia, but there has been little information. The predominant type of glucose transporters for muscle is GLUT-4 and it is known to be insulin dependent [26]. Further evaluation is needed. Muscle FDG uptake may be a good indicator for the differentiation between chronic hyperglycemia due to diabetes and acute hyperglycemia (or normoglycemia) after oral ingestion, because oral ingestion usually effects the FDG accumulation of muscles. Therefore, in case of acute hyperglycemia, muscle FDG uptake would rise according to plasma glucose level and this high muscle uptake might affect the results of oncologic diagnosis.

Limitations of the present study must be mentioned. In the present study, the presence or absence of malignant lesion was confirmed in about half of the cases by other imaging modalities, with clinical follow-ups for at least 6 months. Regarding the mainly targeted tumors (primary lesions), our confirmation was definite in the present study,

Table 4 Cases received for follow-up FDG-PET within 3 months after treatment for diabetes and for cancer

Case no.	Age	Gender	Diagnosis	First FDG-PET SUVmax	Plasma glucose level (mg/dl)	Treatment for cancer Treatment for diabetes	Days after the first PET	Second FDG-PET SUVmax	Plasma glucose level (mg/dl)
1	58	M	Buccal mucosal cancer	Pre-chemotherapy		Neoadjuvant chemotherapy	28 days later	Progressive disease	
5				9.4	235	Insulin injection		9.8	100
2	70	M	Lung cancer	Pre-radiotherapy		Stereotactic radiosurgery	77 days later	Partial remission	
16				3.5	224	Insulin injection		2.6	174
3	42	M	Pancreas cancer	Pre-chemotherapy		Systemic chemotherapy	70 days later	No change	
28				2.3	301	Insulin injection		2.6	115

while additional lesions, such as small lymph nodes or small metastatic lesions, might not be accurately confirmed due to limited information or limitation in the resolution of other imaging modalities. Especially in a case of advanced cancer under chemotherapy, there is no way to confirm such kind of small lesions in the follow-up observation. It cannot be denied that there is a possibility of the presence of more false-negative (probably small) lesions from the pathological point of view. In addition, our PET machine in this study was not a PET/CT. For the diagnostic performance with PET/CT, the results of sensitivity or detectability might be better, especially at the level of SUV 2.0–3.0 (patient#2, 18, 30). Secondly, it was impossible to compare tumor FDG uptake under hyperglycemia to that under normal glucose level in the same patient immediately after treatment for diabetes. Comparison of tumor FDG accumulation between two scans in the same patient under high and normal glucose level would be interesting. There was, however, no patient in the present study who received FDG-PET scans again under normal glucose level after treatment for diabetes without receiving cancer treatment. In our study, there were only three patients who received re-examination of FDG-PET within 3 months after treatment for diabetes and cancer (Table 4). In all cases, the effects of the change in the plasma glucose level after treatment of diabetes were not apparent.

Conclusions

FDG accumulation in the FDG-avid tumor of a certain size (larger than 15 mm) remained high enough for visual diagnosis in the majority of the cases, even under chronic hyperglycemia (more than 200 mg/dl). Under fasting condition with chronic hyperglycemia caused by severe diabetes in this study, diagnostic results showed its sensitivity, specificity and diagnostic accuracy as 83, 83 and 83%, respectively, which is supposed to be almost satisfactory for clinical oncologic diagnosis. Therefore, PET scan can be performed in uncontrolled or untreated diabetic patients under fasting condition, rather than re-examination with FDG-PET at a later date, because re-examination after treatment of diabetes may cause possible delay in treatment, especially in patients with an aggressive cancer, such as pancreatic cancer.

References

1. Bomanji JB, Costa DC, Ell PJ. Clinical role of positron emission tomography in oncology. Lancet Oncol. 2001;3:157–64.
2. Wahl RL, Henry CA, Ethier SP. Serum glucose: effects on tumor and normal tissue accumulation of 2-[F-18]-fluoro-2-deoxy-D-glucose in rodents with mammary carcinoma. Radiology. 1992;183:643–7.
3. Torizuka T, Clavo AC, Wahl RL. Effect of hyperglycemia on in vitro tumor uptake of tritiated FDG, thymidine, L-methionine and L-leucine. J Nucl Med. 1997;38:382–6.
4. Zhao S, Kuge Y, Tsukamoto E, Mochizuki T, Kato T, Hikosaka K, et al. Effects of insulin and glucose loading on FDG uptake in experimental malignant tumours and inflammatory lesions. Eur J Nucl Med. 2001;28:730–5.
5. Lindholm P, Minn H, Leskinen-Kallio S, Bergman J, Ruotsalainen U, Joensuu H. Influence of the blood glucose concentration on FDG uptake in cancer—a PET study. J Nucl Med. 1993;34:1–6.
6. Diederichs CG, Staib L, Glatting G, Beger HG, Reske SN. FDG-PET: elevated plasma glucose reduces both uptake and detection rate of pancreatic malignancies. J Nucl Med. 1998;39:1030–3.
7. Zimny M, Bares R, Fass J, Adam G, Cremerius U, Dohmen B, et al. Fluorine-18 fluorodeoxyglucose positron emission tomography in the differential diagnosis of pancreatic carcinoma: a report of 106 cases. Eur J Nucl Med. 1997;24:678–82.
8. Delbeke D, Coleman RE, Guiberteau MJ, Brown ML, Royal HD, Siegel BA, et al. Procedure guideline for tumor imaging with ^{18}F-FDG PET/CT 1.0. J Nucl Med. 2006;47:885–95.
9. Kitano H, Magata Y, Tanaka A, Mukai T, Kuge Y, Nagatsu K, et al. Performance assessment of O-18 water purifier. Ann Nucl Med. 2001;15:75–8.
10. Gorenberg M, Hallett WA, O'Doherty MJ. Does diabetes affect [(18)F]FDG standardised uptake values in lung cancer? Eur J Nucl Med Mol Imaging. 2002;29:1324–7.
11. Chang YC, Yen TC, Ng KK, See LC, Lai CH, Chang TC, et al. Does diabetes mellitus influence the efficacy of FDG-PET in the diagnosis of cervical cancer? Eur J Nucl Med Mol Imaging. 2005;32:647–52.
12. Hatano E, Ikai I, Higashi T, Teramukai S, Torizuka T, Saga T, et al. Preoperative positron emission tomography with fluorine-18-fluorodeoxyglucose is predictive of prognosis in patients with hepatocellular carcinoma after resection. World J Surgery. 2006;30:1736–41.
13. Higashi T, Saga T, Nakamoto Y, Ishimori T, Fujimoto K, Doi R, et al. Diagnosis of pancreatic cancer using fluorine-18 fluorodeoxyglucose positron emission tomography (FDG PET)—usefulness and limitation in "clinical reality". Ann Nucl Med. 2003;17:261–79.
14. Seo S, Hatano E, Higashi T, Hara T, Tada M, Tamaki N, et al. Fluorine-18 fluorodeoxyglucose positron emission tomography predicts tumor differentiation, P-glycoprotein expression, and outcome after resection in hepatocellular carcinoma. Clin Cancer Res. 2007;13:427–33.
15. Cook GJ, Houston S, Rubens R, Maisey MN, Fogelman I. Detection of bone metastases in breast cancer by 18FDG PET: differing metabolic activity in osteoblastic and osteolytic lesions. J Clin Oncol. 1998;16:3375–9.
16. Mamede M, Higashi T, Kitaichi M, Ishizu K, Ishimori T, Nakamoto Y, et al. [18F]FDG uptake and PCNA, Glut-1, and Hexokinase-II expressions in cancers and inflammatory lesions of the lung. Neoplasia. 2005;7:369–79.
17. Seo S, Hatano E, Higashi T, Nakajima A, Nakamoto Y, Tada M, et al. Fluorine-18 fluorodeoxyglucose positron emission tomography predicts lymph node metastasis, P-glycoprotein expression, and recurrence after resection in mass-forming intrahepatic cholangiocarcinoma. Surgery. 2008;143:769–77.
18. Namageyo-Funa A, Nanavati P. The challenges of addressing primary prevention of diabetes: a response to recommendations from the chronic disease directors' project. J Public Health Manag Pract. 2008;14:26–8.

19. Schiel R, Beltschikow W, Steiner T, Stein G. Diabetes, insulin, and risk of cancer. Methods Find Exp Clin Pharmacol. 2006;28:169–75.
20. Nishikawa T, Edelstein D, Du XL. Normalizing mitochondrial superoxide production blocks three pathways of hyperglycemic damage. Nature. 2000;404:787–90.
21. Guyot LL, Diaz FG, O'Regan MH, Song D, Phillis JW. The effect of topical insulin on the release of excitotoxic and other amino acids from the rat cerebral cortex during streptozotocin-induced hyperglycemic ischemia. Brain Res. 2000;872:29–36.
22. Duelli R, Maurer MH, Staudt R, Heiland S, Duembgen L, Kuschinsky W. Increased cerebral glucose utilization and decreased glucose transporter Glut-1 during chronic hyperglycemia in rat brain. Brain Res. 2000;858:338–47.
23. Alpert E, Gruzman A, Totary H, Kaiser N, Reich R, Sasson S. A natural protective mechanism against hyperglycemia in vascular endothelial and smooth-muscle cells: role of glucose and 12-hydroxyeicosatetraenoic acid. Biochem J. 2002;362:413–22.
24. Nagamatsu S, Sawa H, Wakizaka A, Hoshino T. Expression of facilitative glucose transporter isoforms in human brain tumors. J Neurochem. 1993;61:2048–53.
25. Peiró C, Lafuente N, Matesanz N, Cercas E, Llergo JL, Vallejo S, et al. High glucose induces cell death of cultured human aortic smooth muscle cells through the formation of hydrogen peroxide. Br J Pharmacol. 2001;133:967–74.
26. Ishiki M, Klip A. Minireview: recent developments in the regulation of glucose transporter-4 traffic: new signals, locations, and partners. Endocrinology. 2005;146:5071–8.

European Journal of Radiology xxx (2009) xxx–xxx

Contents lists available at ScienceDirect

European Journal of Radiology

journal homepage: www.elsevier.com/locate/ejrad

Non-contrast-enhanced hepatic MR angiography: Do two-dimensional parallel imaging and short tau inversion recovery methods shorten acquisition time without image quality deterioration?

Kotaro Shimada*, Hiroyoshi Isoda, Tomohisa Okada, Toshikazu Kamae, Shigeki Arizono, Yuusuke Hirokawa, Toshiya Shibata, Kaori Togashi

Department of Diagnostic Imaging and Nuclear Medicine, Kyoto University, Graduate School of Medicine, 54 Kawahara-cho, Shogoin, Sakyo-ku, Kyoto 606-8507, Japan

ARTICLE INFO

Article history:
Received 12 April 2009
Accepted 28 May 2009

Keywords:
Hepatic artery
Magnetic resonance angiography
Non-contrast-enhanced
Time spatial labeling inversion pulse
Two-dimensional parallel imaging
Short tau inversion recovery

ABSTRACT

Objective: To study whether shortening the acquisition time for selective hepatic artery visualization is feasible without image quality deterioration by adopting two-dimensional (2D) parallel imaging (PI) and short tau inversion recovery (STIR) methods.

Materials and methods: Twenty-four healthy volunteers were enrolled. 3D true steady-state free-precession imaging with a time spatial labeling inversion pulse was conducted using 1D or 2D-PI and fat suppression by chemical shift selective (CHESS) or STIR methods. Three groups of different scan conditions were assigned and compared: group A (1D-PI factor 2 and CHESS), group B (2D-PI factor 2 × 2 and CHESS), and group C (2D-PI factor 2 × 2 and STIR). The artery-to-liver contrast was quantified, and the quality of artery visualization and overall image quality were scored.

Results: The mean scan time was 9.5 ± 1.0 min (mean ± standard deviation), 5.9 ± 0.8 min, and 5.8 ± 0.5 min in groups A, B, and C, respectively, and was significantly shorter in groups B and C than in group A ($P < 0.01$). The artery-to-liver contrast was significantly better in group C than in groups A and B ($P < 0.01$). The scores for artery visualization and overall image quality were worse in group B than in groups A and C. The differences were statistically significant ($P < 0.05$) regarding the arterial branches of segments 4 and 8. Between group A and group C, which had similar scores, there were no statistically significant differences.

Conclusion: Shortening the acquisition time for selective hepatic artery visualization was feasible without deterioration of the image quality by the combination of 2D-PI and STIR methods. It will facilitate using non-contrast-enhanced MRA in clinical practice.

1. Introduction

Selective visualization of the hepatic artery with MR angiography (MRA) without using a contrast-enhancing agent has great clinical significance in patients with decreased renal function or allergies to contrast agents. Recently, the capability of non-contrast-enhanced MRA for depicting the hepatic artery was demonstrated by the combined usage of a respiratory-triggered three-dimensional (3D) true steady-state free-precession (SSFP) sequence and a time spatial labeling inversion pulse (T-SLIP) [1]. The true SSFP sequence is based on a gradient-echo sequence in which the gradients are fully balanced without spoiling transverse magnetization, and the signal-to-noise ratio (SNR) is relatively high even without using a contrast agent [2]. Steady-state signal is dependent on T2-to-T1 ratio that is relatively high for blood and true SSFP acquisition has been used successfully for vascular imaging [3,4]. The T-SLIP is a kind of spin labeling pulse, which can be placed anywhere, independent of imaging area, and is used for selective signal suppression of the background or vessels of no interest. It also provides selective inflow information by the setting of an appropriate inversion time (TI) [5].

In a previous study, high contrast visualization of the hepatic artery was obtained while signals from other vessels and static tissues were adequately suppressed [1]. However, the acquisition took up to 10 min, which is too long for clinical use. In addition, long acquisition may cause motion artifacts and lead to deterioration of image quality. Shortening of the acquisition time is feasible using the parallel imaging (PI) method. In the former study, a

* Corresponding author. Tel.: +81 75 751 3760; fax: +81 75 771 9709.
E-mail addresses: kotaro@kuhp.kyoto-u.ac.jp (K. Shimada), sayuki@kuhp.kyoto-u.ac.jp (H. Isoda), tomokada@kuhp.kyoto-u.ac.jp (T. Okada), toshi13@kuhp.kyoto-u.ac.jp (T. Kamae), arizono@kuhp.kyoto-u.ac.jp (S. Arizono), yuusuke@kuhp.kyoto-u.ac.jp (Y. Hirokawa), ksj@kuhp.kyoto-u.ac.jp (T. Shibata), ktogashi@kuhp.kyoto-u.ac.jp (K. Togashi).

0720-048X/$ – see front matter © 2009 Elsevier Ireland Ltd. All rights reserved.
doi:10.1016/j.ejrad.2009.05.051

Please cite this article in press as: Shimada K, et al. Non-contrast-enhanced hepatic MR angiography: Do two-dimensional parallel imaging and short tau inversion recovery methods shorten acquisition time without image quality deterioration? Eur J Radiol (2009), doi:10.1016/j.ejrad.2009.05.051

one-dimensional (1D) PI with a factor of 2 in the phase-encoding direction was used, but two-dimensional (2D) PI can be used to further decrease the scan time, although a concurrent decrease in SNR may exacerbate the image quality [6,7].

One of the solutions to this problem is greater reduction of the background signal. In this study, we used the short tau inversion recovery (STIR) method in combination with a T-SLIP for larger background signal suppression in order to compensate for the signal decrease induced by 2D-PI. In a STIR sequence, an inversion pulse is applied and a short period of time is allowed for the nullification of the longitudinal magnetization of fat [8]. The acquired signal reflects the absolute value of the longitudinal magnitude of the spins in a tissue. Fat has one of the shortest T1 values in the abdominal region, and the liver parenchyma also has a relatively short T1 value compared with arterial blood [9]. This means that the addition of the STIR method to a T-SLIP may contribute to further suppression of the background signal and facilitate improved visualization of the hepatic artery.

Hence, we hypothesized that shortening of the acquisition time for non-contrast-enhanced visualization of the hepatic artery is feasible without deteriorating image quality by combined usage of the 2D-PI and STIR methods.

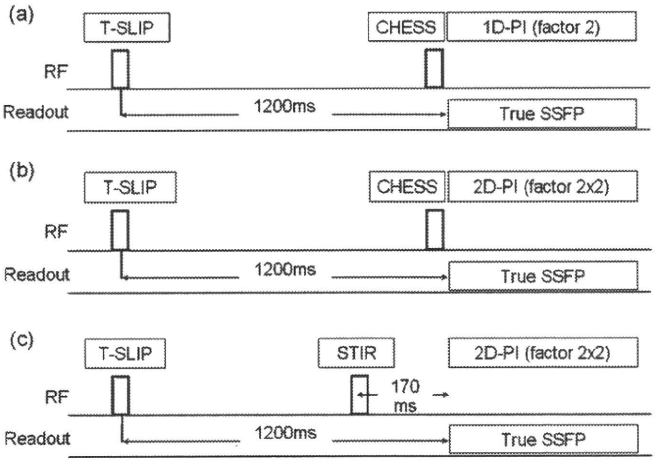

Fig. 1. Illustrations of the three different scan conditions. (a) In group A, 1D parallel imaging (PI) with a factor of 2 in the phase-encoding direction and a CHESS pulse for fat saturation were used. (b) In group B, 2D-PI with factors of 2 × 2 in the phase and slice-encoding direction and a CHESS pulse were used. (c) In group C, 2D-PI with factors of 2 × 2 and a STIR pulse for fat suppression were used. Parallel imaging applied in the slice direction reduced scan time.

2. Materials and methods

2.1. Subjects

This study was approved by our institutional review board and was conducted in accordance with the ethical standards of the World Medical Association (Declaration of Helsinki). Twenty-four healthy adult subjects (16 males and 8 females, mean age: 27 years, range: 19–45 years old) were included in this study. Written informed consent was obtained from all subjects before MRI examinations.

2.2. MR imaging

All examinations were conducted using a 1.5 T MRI system (EXCELART Vantage, powered by Atlas; Toshiba Medical Systems, Otawara, Japan), equipped with a pair of phased array coils containing 16 active coil elements connected to 16 receiver channels, which were placed at the front and back of the abdomen. After obtaining scout images in three orthogonal planes, coronal true SSFP images without an inversion pulse were acquired [repetition time (TR)/echo time (TE) = 5.2/2.6 ms, flip angle = 70°, field-of-view (FOV) = 400 mm × 400 mm, matrix = 256 × 256, number of slices = 16, slice thickness = 10 mm, scanning time = 12 s] to localize the abdominal aorta, celiac trunk, and liver.

For visualization of the hepatic arterial system, 3D true SSFP imaging with a T-SLIP was conducted in the coronal plane. Respiratory-triggering and fat saturation methods were applied. The respiratory-triggering signal was produced at the mid-point of expiration using a bellows wrapped around the abdomen to reduce motion artifacts. The chemical shift selective (CHESS) or STIR methods (TI = 170 ms) were used for fat suppression, and 1D or 2D-PI was used to allow shorter acquisition. Imaging of the hepatic artery was conducted in three different conditions, designated as groups A, B, and C (Fig. 1). In group A, a CHESS pulse and 1D-PI in the phase-encoding direction with a factor of 2 were used, which was the same as in the former study [1] and was used as a reference standard. In group B, a CHESS pulse and 2D-PI in both phase and slice encoding directions with factors of 2 and 2, respectively, were applied. In group C, a SITR pulse and the same 2D-PI as in group B were used.

Common scan parameters were TR/TE/FA = 4.3 ms/2.2 ms/120°, receiver bandwidth of 781 Hz/pixel, FOV = 400 mm × 300 mm, matrix size = 256 × 256, slice thickness = 1.5 mm, number of slices = 60, and number of acquisition = 1. The spatial resolution was 1.6 mm × 1.2 mm × 1.5 mm, and the final images were reconstructed into an apparent spatial resolution of 0.6 mm × 0.6 mm × 0.75 mm by zero filling. The order of phase encoding was centric in all groups. All subjects were instructed to breathe regularly during the scan.

2.3. Application of a T-SLIP

A T-SLIP of 25 cm-width was placed on the abdomen in order to cover the liver, gallbladder, and portal venous system and to suppress their signals (Fig. 2). The superior border of the inversion pulse was placed parallel to the line of the upper liver edge and near the celiac trunk (approximately 2 cm cranial to it) in order to

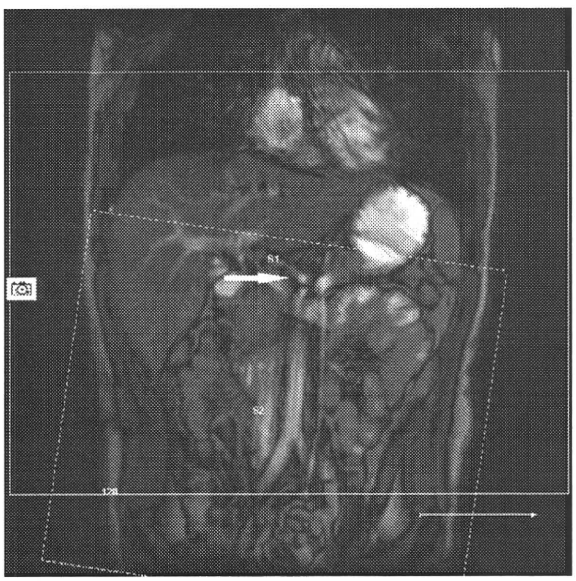

Fig. 2. T-SLIP placement on a scout image. The superior border of the inversion pulse (dotted lines) was placed approximately 2 cm cranial to the celiac trunk (arrow). As a result, the inflowing blood signal of the descending aorta arrived immediately into the hepatic artery, and good vessel visualization without background signal recovery was obtained. The imaging area is indicated with solid lines.

Please cite this article in press as: Shimada K, et al. Non-contrast-enhanced hepatic MR angiography: Do two-dimensional parallel imaging and short tau inversion recovery methods shorten acquisition time without image quality deterioration? Eur J Radiol (2009), doi:10.1016/j.ejrad.2009.05.051

allow inflowing arterial blood to reach the hepatic artery with minimal signal saturation. The TI value was fixed at 1200 ms, which was adopted from a previous study [1].

2.4. Imaging analysis

Three image groups, A (1D-PI factor 2 and CHESS), B (2D-PI factor 2 × 2 and CHESS), and C (2D-PI factor 2 × 2 and STIR), were analyzed and statistically compared. Maximum intensity projection (MIP) reconstructions were used in addition to the source images. Quantitative analysis was conducted by a radiologist (K.S. with 9 years of experience), and qualitative analysis was performed in consensus by two experienced radiologists (H.I. with 19 years of experience and K.S. with 9 years of experience), who were blinded to the names, personal data, and scan parameters of the subjects. If there was a disagreement between the two reviewers, a third radiologist (T.O. who has 20 years of experience) made a final decision. All quantitative and qualitative assessments of image quality were performed on a commercially available workstation (Ziostation, Ziosoft, Tokyo, Japan).

2.4.1. Quantitative evaluation

The means and standard deviations (S.D.) of the acquisition time were calculated and compared. The signal intensity (SI) of the right hepatic artery (RHA) was compared with that of the surrounding liver parenchyma as a reference tissue by placing regions-of-interest (ROI) because S.D. of the background noise signal could not be used to calculate SNR due to the use of the PI method [10]. The sizes of the ROI in the RHA were 5–10 mm^2 and those in the liver were at least 40 mm^2 and chosen in homogenous, artifact-free areas adjacent to the RHA. These values were used to calculate the artery-to-liver contrast (Ca-l) with the following equation: Ca-l = (SI_artery–SI_liver)/SI_artery [1].

2.4.2. Qualitative evaluation

The visualization quality was scored on a four-point scale (1 = not visible and non-diagnostic image quality, 2 = poor image quality without sufficient visualization, 3 = good image quality sufficient for diagnosis, and 4 = excellent image quality with sharply defined hepatic arteries) for assessment of the RHA, left hepatic artery (LHA), and arterial branches of segment 4 (A4) and segment 8 (A8). In addition, the evaluators were asked to score overall image quality based on the degree of whole artery visualization, motion artifacts, and signal suppression of the background, especially of the biliary and gastrointestinal tracts using a three-point scale (1 = poor artery visualization with severe motion artifacts, insufficient background signal suppression, or both, 2 = sufficient artery visualization despite motion artifacts or a residual background signal, 3 = good artery visualization with little or no motion artifacts and good background signal suppression).

2.5. Statistical analysis

Statistical analyses were conducted using a commercially available software package (Statview, version 5.0.1; SAS Institute, Cary, USA). The artery-to-liver contrast and the acquisition time of each group were compared using one-way repeated-measures analysis of variance (ANOVA) followed by the post hoc test. The qualitative results of the three different protocol groups were compared using Friedman's nonparametric test and Scheffe's test. A *P*-value of less than 0.05 was considered to indicate a statistically significant difference.

Table 1
The means and standard deviations of scan times, quantitative and qualitative results.

	Group A (1D-PI factor 2 and CHESS)	Group B (2D-PI factor 2 × 2 and CHESS)	Group C (2D-PI factor 2 × 2 and STIR)
Scan time (min)	9.5 ± 1.0	5.9 ± 0.8[a]	5.8 ± 0.5[a]
Ca-l	0.61 ± 0.08	0.59 ± 0.11	0.80 ± 0.07[b]
Visualization scores			
RHA	3.8 ± 0.5	3.6 ± 0.6	3.8 ± 0.6
LHA	3.8 ± 0.5	3.6 ± 0.7	3.7 ± 0.6
A4	3.1 ± 0.8[c]	2.5 ± 0.6	3.2 ± 0.6[c]
A8	3.3 ± 0.8[c]	2.7 ± 0.8	3.3 ± 0.7[c]
Overall image quality	2.9 ± 0.2	2.6 ± 0.5	2.9 ± 0.3

Ca-l, artery-to-liver contrast; RHA, right hepatic artery; LHA, left hepatic artery; A4, arterial branch of segment 4; A8, arterial branch of segment 8; 1D, one-dimensional; 2D, two-dimensional; PI, parallel imaging; CHESS, chemical shift selective; STIR, short tau inversion recovery.

[a] Significantly shorter than group A ($P < 0.01$).

[b] Significantly higher than groups A and B ($P < 0.01$).

[c] Significantly better than group B ($P < 0.05$).

3. Results

3.1. Quantitative analysis

Imaging was successfully performed in all subjects. The acquisition times were 9.5 ± 1.0 min (mean ± S.D.), 5.9 ± 0.8 min, and 5.8 ± 0.5 min in groups A, B, and C, respectively (Table 1), and were significantly shorter in groups B and C than in group A ($P < 0.01$). There was no significant difference in the acquisition time between groups B and C ($P > 0.05$). The means and standard deviations of the artery-to-liver contrast were 0.61 ± 0.08, 0.59 ± 0.11, and 0.80 ± 0.07 for groups A, B, and C, respectively (Table 1). In group C, the Ca-l was significantly better than in the other groups ($P < 0.01$) due to good signal suppression of the background (Figs. 3–5). There was no significant difference between groups A and B ($P > 0.05$).

3.2. Qualitative analysis

The scores for visualization quality and overall image quality in each group are summarized in Table 1. The image quality scores of the RHA, LHA, A4, and A8 were all lower in group B than in the other groups. Regarding A4 and A8 visualization, the differences were statistically significant ($P < 0.05$). As for overall image quality, group B was worse than the other groups, but there were no significant differences (Figs. 3–5). In any of the evaluated parameters, there were no significant differences between group A and group C.

4. Discussion

The accurate assessment of hepatic arterial anatomy is essential for patients who are being considered for liver resection or transplantation [11–13]. Multi-detector row 3D CT angiography provides excellent vascular detail and is one of the most important methods for the assessment of liver anatomy, due to its accessibility and brief scan time [14]. On the other hand, contrast-enhanced MR angiography has been established as a valuable method for detecting vascular disease without radiation exposure [15,16]. However, both CT and MR contrast agents have some risk of contrast-medium-induced nephropathy and other adverse effects, including rare but lethal reactions such as anaphylactic shock and nephrogenic systemic fibrosis [17,18]. Thus, selective visualization of the hepatic artery with non-contrast-enhanced MRA would be beneficial for some patients, especially those that suffer from nephropathy.

Please cite this article in press as: Shimada K, et al. Non-contrast-enhanced hepatic MR angiography: Do two-dimensional parallel imaging and short tau inversion recovery methods shorten acquisition time without image quality deterioration? Eur J Radiol (2009), doi:10.1016/j.ejrad.2009.05.051

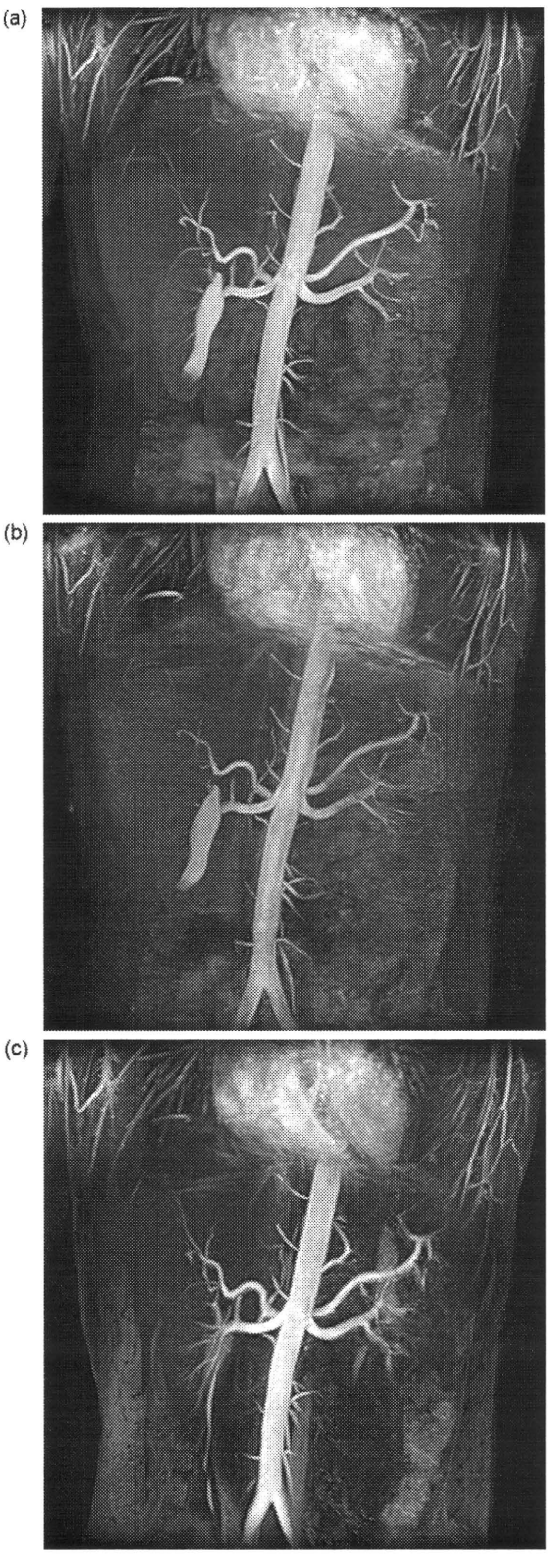

Fig. 3. Coronal MIP images of a 20-year-old subject in group A (a), group B (b), and group C (c). Signal of the liver parenchyma is better suppressed in group C than in the other groups. No motion artifacts are conspicuous in any group.

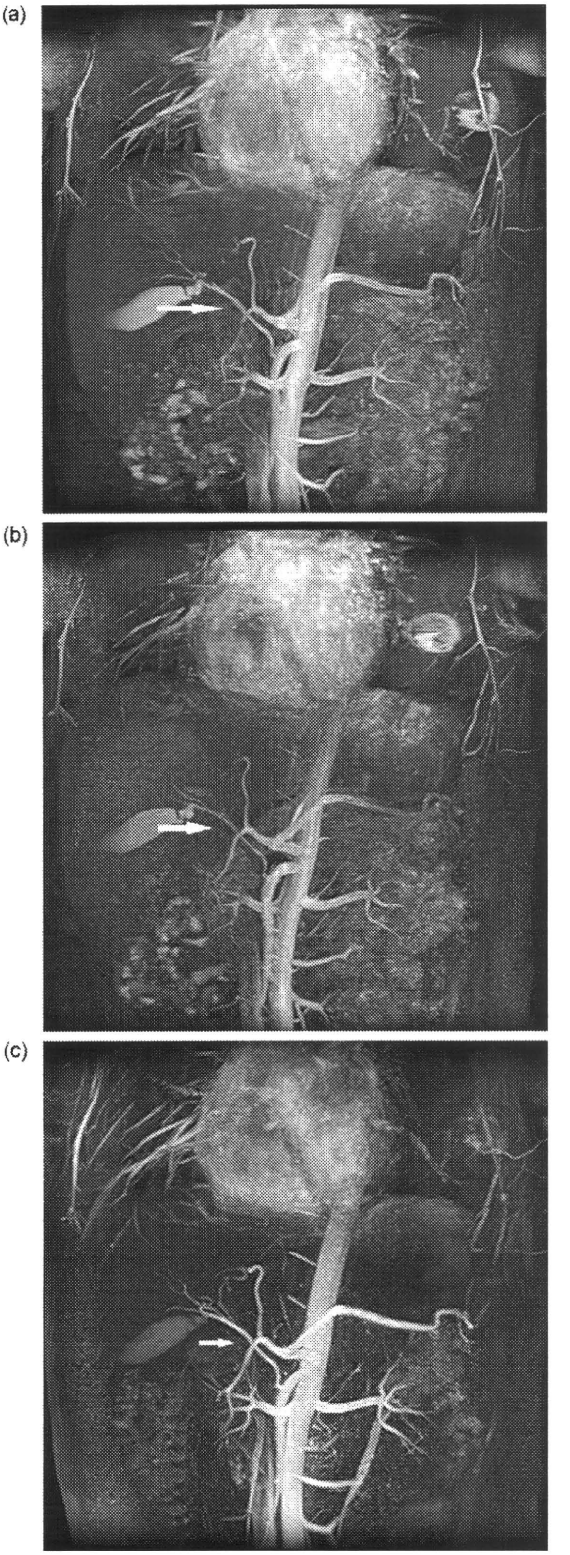

Fig. 4. Coronal MIP images of a 35-year-old subject in group A (a), group B (b), and group C (c). In group C, signals of the gallbladder and intestinal fluid, as well as the liver parenchyma, are well suppressed. The peripheral hepatic artery including A8 is better visualized in groups A and C than in group B. The replaced right hepatic artery arising from the superior mesenteric artery is well depicted in all groups (arrow).

In our previous study, we successfully demonstrated that the combination of a respiratory-triggered 3D true SSFP sequence and the T-SLIP technique enabled selective hepatic artery visualization during free breathing and without the need for an exogenous contrast agent [1]. However, the acquisition time, which ranged from

Please cite this article in press as: Shimada K, et al. Non-contrast-enhanced hepatic MR angiography: Do two-dimensional parallel imaging and short tau inversion recovery methods shorten acquisition time without image quality deterioration? Eur J Radiol (2009), doi:10.1016/j.ejrad.2009.05.051

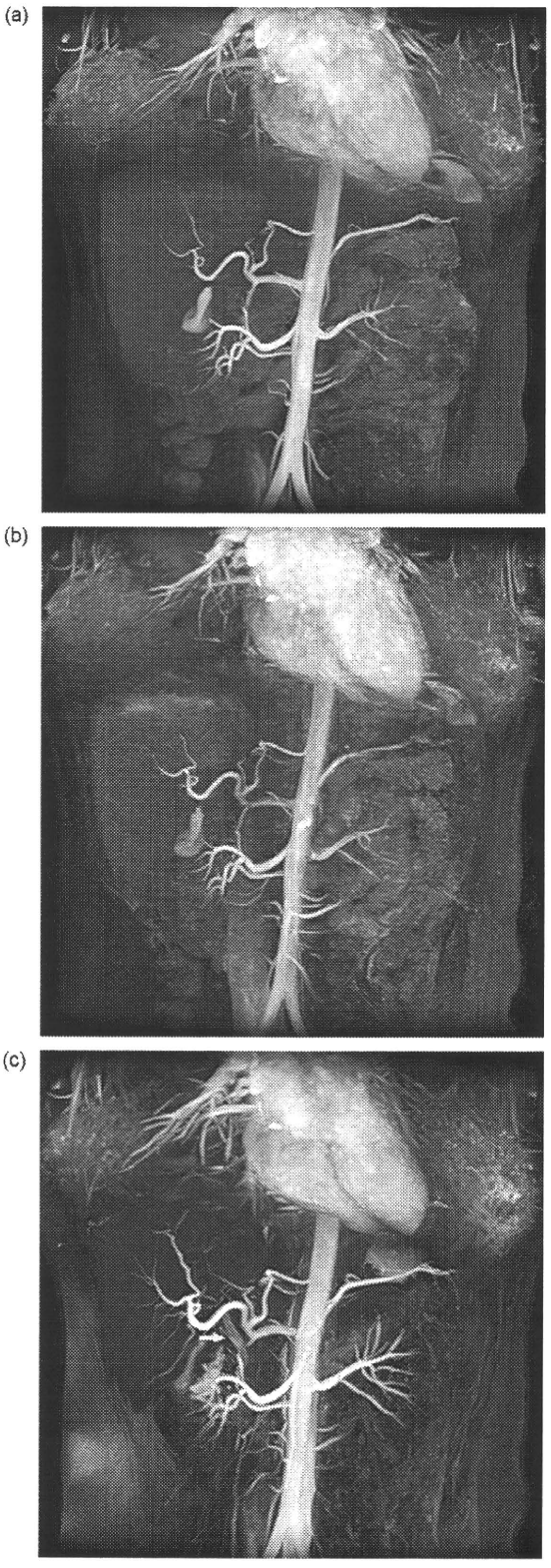

Fig. 5. Coronal MIP images of a 23-year-old subject in group A (a), group B (b), and group C (c). Distal arterial branches are clearly visible in group C, but the biliary tract is also prominent, probably due to serous bile, which has a long T1 value (arrow).

6 to 10 min, was too long and needs to be shortened before the clinical use of this method. One of the ways to obtain a shorter acquisition time is to increase the PI factor, but this may result in a large increase in the g-factor, and the image is degraded more than the attained acceleration when it is applied in only one direction [6]. Therefore, we adopted the 2D-PI method, and the mean scan time was significantly reduced from 10 to 6 min.

The reason we used STIR was not only to obtain complete fat suppression, but also to obtain good image quality by suppressing the surrounding tissues with short T1 values, including the liver parenchyma, gastrointestinal tract, and gallbladder [19]. The combination of the PI and STIR techniques that we used in this study successfully shortened the acquisition time for selective hepatic artery visualization without marked deterioration of the image quality. Shortening the acquisition time will decrease the burden on the patient, and make the method more comfortable and suitable for clinical use.

Strong signal suppression of the background, especially that of the liver parenchyma, was obtained by the STIR technique in group C, and it led to better Ca-I than the other groups in quantitative analyses. The relatively short T1 of the liver parenchyma compared with the arterial blood may lead to a better contrast between the hepatic artery and liver parenchyma by the STIR technique. Also, regarding qualitative analyses, the image quality scores were almost identical in group A (reference standard) and group C, but these scores were lower in group B, and there were statistically significant differences between group B and the other groups regarding the visualization of A4 and A8 ($P < 0.05$). The improved contrast between the hepatic artery and liver parenchyma in group C may compensate for the decrease in SNR accompanied by the increase of PI factor and may lead to better peripheral artery visualization compared with group B.

The visualization scores of the RHA and LHA were near to the maximum scores; however, the visualization of A4 and A8, which represent smaller branches, was still insufficient and needs to be higher. One of the limitation factors for better peripheral visualization would be the arterial flow itself. A longer TI of the T-SLIP, such as 1400 ms, may allow arterial flow to reach more peripheral areas, but in the previous study, concurrent background signal recovery exacerbated the image quality [1]. However, the STIR technique we used in this study strongly suppressed the background signal, so better peripheral visualization of the hepatic artery may be feasible using a longer TI of the T-SLIP.

No motion artifacts were conspicuous in any group, probably owing to our prior explanation to breathe regularly (Figs. 3–5). The short T1 values of concentrated bile in the gallbladder and intestinal fluid contributed to the improved signal suppression by a STIR pulse in group C compared with groups A and B, which used a CHESS pulse (Figs. 3 and 4). In contrast, serous fluid in the biliary tract, which usually has a longer T1 value, was more conspicuous after the use of the STIR method in group C, probably due to greater background signal suppression (Fig. 5).

The acquisition time of our method is still much longer than that of contrast-enhanced CT and MRI, in which only a single breath hold is usually required for data acquisition. However, optimal timing is crucial for these acquisitions, and when sufficient image quality is not obtained for such reasons as reduced breath-hold capability or gross body movement, the rescanned image is usually much degraded [20]. In contrast, the proposed method can be retried at the sole expense of 6 min. Furthermore, this relatively long scan time is acceptable when the preparation time for contrast enhancement and possible adverse effects is taken into consideration.

A limitation of this study is the absence of a solid reference standard. Instead in this study, a previously reported acquisition method was used as a reference standard, which may be sufficient to compare three imaging sequences. Another issue is the subject

Please cite this article in press as: Shimada K, et al. Non-contrast-enhanced hepatic MR angiography: Do two-dimensional parallel imaging and short tau inversion recovery methods shorten acquisition time without image quality deterioration? Eur J Radiol (2009), doi:10.1016/j.ejrad.2009.05.051

population. No patient was included in this study, but it may not be necessary for the purpose of this study.

In conclusion, the combination of 2D-PI and STIR methods enabled faster acquisition without impairing visualization quality. This improved technical approach is considered applicable to clinical use, especially for patients with renal hypofunction or allergies to contrast agents.

Acknowledgments

This study was conducted as a part of the project, "R&D of Molecular Imaging Equipment for Malignant Tumor Therapy Support," supported by NEDO (New Energy and Industrial Technology Development Organization), Japan. The author thanks Toshie Chiba, Saori Satou, and Ayako Ninomiya (Toshiba Medical Systems) for their excellent technical assistance and all volunteers who were willing to participate in our study.

References

[1] Shimada K, Isoda H, Okada T, et al. Non-contrast-enhanced hepatic MR angiography with true steady-state free-precession and time spatial labeling inversion pulse: optimization of the method and preliminary results. Eur J Radiol 2008, doi:10.1016/j.ejrad.2007.12.010 [February 2, Epub.].
[2] Shimada K, Isoda H, Okada T, et al. Non-contrast-enhanced MR angiography for selective visualization of the hepatic vein and inferior vena cava with true steady-state free-precession sequence and time-spatial labeling inversion pulses: preliminary results. J Magn Reson Imaging 2009;29(2):474–9.
[3] Ito K, Koike S, Jo C, et al. Intraportal venous flow distribution: evaluation with single breath-hold ECG-triggered three-dimensional half-Fourier fast spin-echo MR imaging and a selective inversion-recovery tagging pulse. AJR 2002;178(2):343–8.
[4] Miyazaki M, Sugiura S, Tateishi F, Wada H, Kassai Y, Abe H. Non-contrast-enhanced MR angiography using 3D ECG-synchronized half-Fourier fast spin echo. J Magn Reson Imaging 2000;12(5):776–83.
[5] Nishimura DG, Macovski A, Jackson JI, Hu RS, Stevick CA, Axel L. Magnetic resonance angiography by selective inversion recovery using a compact gradient echo sequence. Magn Reson Med 1988;8(1):96–103.
[6] Weiger M, Pruessmann KP, Boesiger P. 2D SENSE for faster 3D MRI. MAGMA 2002;14(1):10–9.
[7] Okada T, Kanao S, Ninomiya A, Sato S, Kuhara S, Kamae T, Gotoh K, Togashi K. Whole-heart coronary magnetic resonance angiography with parallel imaging: comparison of acceleration in one-dimension vs. two-dimensions. Eur J Radiol 2008, doi:10.1016/j.ejrad.2008.06.005 [July 19, Epub.].
[8] Delfaut EM, Beltran J, Johnson G, Rousseau J, Marchandise X, Cotten A. Fat suppression in MR imaging: methods and pitfalls. Radiographics 1999;19(2):373–82.
[9] Bernstein MA, King FK, Zhou XJ. Handbook of MRI pulse sequences. London, UK: Elsevier Academic Press; 2004, 960–962.
[10] Xu PJ, Yan FH, Wang JH, et al. Utilizing generalized autocalibrating partial parallel acquisition (GRAPPA) to achieve high-resolution contrast-enhanced MR angiography of hepatic artery: initial experience in orthotopic liver transplantation candidates. Eur J Radiol 2007;61(3):507–12.
[11] Ralls PW. Color Doppler sonography of the hepatic artery and portal venous system. AJR Am J Roentgenol 1990;155(3):517–25.
[12] Yalavarthy R, Edelstein CL, Teitelbaum I. Acute renal failure and chronic kidney disease following liver transplantation. Hemodial Int 2007;11(Suppl. 3):S7–12.
[13] Moreau R, Lebrec D. Diagnosis and treatment of acute renal failure in patients with cirrhosis. Best Pract Res Clin Gastroenterol 2007;21(1):111–23.
[14] Kang HK, Jeong YY, Choi JH, et al. Three-dimensional multidetector row CT portal venography in the evaluation of porto-systemic collateral vessels in liver cirrhosis. Radiographics 2002;22(5):1053–61.
[15] Kreft B, Strunk H, Flacke S, et al. Detection of thrombosis in the portal venous system: comparison of contrast-enhanced MR angiography with intraarterial digital subtraction angiography. Radiology 2000;216(1):86–92.
[16] Ito K, Blasbalg R, Hussain SM, et al. Portal vein and its tributaries: evaluation with thin-section three-dimensional contrast-enhanced dynamic fat-suppressed MR imaging. Radiology 2000;215(2):381–6.
[17] Thomsen HS, Morcos SK. Contrast-medium-induced nephropathy: is there a new consensus? A review of published guidelines. Eur Radiol 2006;16(8):1835–40.
[18] Dawson P. Nephrogenic systemic fibrosis: possible mechanisms and imaging management strategies. J Magn Reson Imaging 2008;28(4):797–804.
[19] Takahara T, Imai Y, Yamashita T, Yasuda S, Nasu S, Van Cauteren M. Diffusion weighted whole body imaging with background body signal suppression (DWIBS): technical improvement using free breathing, STIR and high resolution 3D display. Radiat Med 2004;22(4):275–82.
[20] Maki JH, Chenevert TL, Prince MR. Contrast-enhanced MR angiography. Abdom Imaging 1998;23(5):469–84.

Please cite this article in press as: Shimada K, et al. Non-contrast-enhanced hepatic MR angiography: Do two-dimensional parallel imaging and short tau inversion recovery methods shorten acquisition time without image quality deterioration? Eur J Radiol (2009), doi:10.1016/j.ejrad.2009.05.051

Unenhanced MR Portography With a Half-Fourier Fast Spin-Echo Sequence and Time–Space Labeling Inversion Pulses: Preliminary Results

Kotaro Shimada[1]
Hiroyoshi Isoda
Tomohisa Okada
Toshikazu Kamae
Shigeki Arizono
Yuusuke Hirokawa
Kaori Togashi

OBJECTIVE. For this study, we aimed to selectively visualize the intrahepatic portal veins using 3D half-Fourier fast spin-echo (FSE) MR angiography (MRA) with a time–space labeling inversion pulse (T-SLIP) and to optimize the acquisition protocol.

SUBJECTS AND METHODS. Respiratory-triggered 3D half-Fourier FSE scans were obtained in 25 healthy adult subjects combined with two different T-SLIPs: one placed on the liver and the thorax to suppress signals of the liver parenchyma, hepatic veins, and abdominal arteries and the other on the lower abdomen to suppress the ascending signal of the inferior vena cava. One of the most important factors was the inversion time (TI) of the inversion pulse for the liver and thorax. Image quality was evaluated in terms of signal-to-noise ratio, contrast-to-noise ratio, and mean visualization scores at four different TIs: 800, 1,200, 1,600, and 2,000 milliseconds.

RESULTS. Selective visualization of the portal vein was successfully achieved in all volunteers, and anatomic variations were also seen in three subjects. A TI of 1,200 milliseconds was optimal in our protocol because it was sufficient for peripheral portal vein visualization and was most suitable for signal suppression of the hepatic veins and liver parenchyma.

CONCLUSION. Half-Fourier FSE scanning with T-SLIPs enabled selective visualization of the portal vein without an exogenous contrast agent.

Keywords: liver, MR angiography, MR portography, MR pulses, MR technique, portal vein, T-SLIP

DOI:10.2214/AJR.08.1626

Received August 2, 2008; accepted after revision January 1, 2009.

This study was conducted as a part of the project "R&D of Molecular Imaging Equipment for Malignant Tumor Therapy Support" and was supported by the New Energy and Industrial Technology Development Organization, Japan.

[1]All authors: Department of Diagnostic Imaging and Nuclear Medicine, Kyoto University Graduate School of Medicine, 54 Kawahara-cho, Shogoin, Sakyo-ku, Kyoto 606-8507, Japan. Address correspondence to K. Shimada (kotaro@kuhp.kyoto-u.ac.jp).

AJR 2009; 193:106–112

0361–803X/09/1931–106

Precise delineation of the portal venous anatomy is essential when assessing patients before hepatectomy or liver transplantation [1]. Contrast-enhanced angiography with CT or MRI is a standard and noninvasive procedure for this purpose [2, 3]. However, both CT and MR contrast agents have side effects, such as anaphylactic shock. In addition, they should not be administered to patients with decreased renal function [4].

Recently, unenhanced MR angiography (MRA) techniques, such as 3D half-Fourier fast spin-echo (FSE) and true steady-state free precession (SSFP), have allowed rapid progress and are being effectively used for visualization of the coronary arteries, renal arteries, and peripheral vessels [5–7]. Unenhanced visualization of the hepatic artery has recently been reported [8]; however, for the portal vein, analysis of only intraportal blood flow distribution has been reported [9]. Those investigators used a half-Fourier FSE technique to make the most of the T2 blurring effect [10] and near-the-center-of-k-space acquisition. The 3D half-Fourier FSE method is one of the new MRA techniques that allows selective visualization of fluid components (i.e., blood) in arteries and veins. In general, an FSE sequence uses a long TE value and shows rapid blood flow as signal void; however, reduced echo-train spacing enables compact echo sampling and reduces this phenomenon, especially when the flow velocity is low, as in the vein [6]. This technique can show slow blood flow, such as portal venous flow, as high signal intensity without the use of a gadolinium-based contrast agent. However, with this technique alone, it is difficult to visualize the portal vein selectively because of overlaps of the hepatic arterial and venous systems.

The time–space labeling inversion pulse (T-SLIP) method is a form of spin labeling that can provide quantitative and selective inflow information by placing the inversion pulse before data acquisition and suppressing the background [11]. A T-SLIP can also be used for selective suppression of the blood signal when it is placed on a vessel of no interest. More than one T-SLIP can be placed arbitrarily independent of the imaging area,

and the T-SLIP method enables selective visualization of the vessel of interest. By changing the inversion time (TI), the T-SLIP method can control the extent of the inflowing blood signal.

To date, the use of unenhanced MRA for selective visualization of the intrahepatic portal system has not been fully evaluated. The purpose of our study was to selectively visualize the portal vein using respiratory-triggered 3D half-Fourier FSE imaging with T-SLIPs and to determine the optimal protocol for its visualization. Herein, we report our initial experience.

Subjects and Methods

Subjects

This study was conducted in accordance with the ethical standards of the World Medical Association (Declaration of Helsinki). From April 2008 to June 2008, 25 healthy adult subjects (18 men and seven women; average age, 28 years; age range, 18–44 years) were included in this study. Institutional review board approval and written informed consent from all subjects were obtained before MRI examinations. All subjects were instructed to breathe normally during scanning.

MRI Protocol

Each examination was conducted with the subject in the supine position using a 1.5-T MRI system (EXCELART Vantage powered by Atlas, Toshiba Medical Systems) equipped with a pair of 4 × 4 phased-array coils placed at both the front and back of the abdomen. Two rows were used for both the front and back coils, resulting in 16 active coil elements connected to 16 receiver channels.

To localize the heart and liver for placement of two different T-SLIPs, coronal true SSFP images without an inversion pulse were acquired using the following parameters: TR/TE, 5.2/2.6; flip angle, 65°; field of view, 400 × 400 mm; matrix, 256 × 256; number of slices, 16; and slice thickness, 10 mm. To visualize the intrahepatic portal venous system selectively, respiratory-triggered 3D single-shot half-Fourier FSE images with fat saturation were acquired in the coronal plane using two T-SLIPs (a work-in-progress sequence from the vendor) at different locations and with a different TI as described in the next section.

Respiratory triggering was conducted at the beginning of expiration using a bellows wrapped around the patient's abdomen to reduce motion artifacts. The scanning parameters were as follows: 1 respiration interval/80; flip angle, 90°; echo-train spacing, 5 milliseconds; slice thickness, 3 mm; number of slices, 35 and no gap; field of view, 370 × 400 mm; receiver bandwidth, 651 Hz/pixel; matrix size, 256 × 256; number of acquisitions, 1; and parallel imaging factor of 2 in the phase direction, resulting in the collection of 128 phase-encoding lines per respiratory trigger in a centric order.

The final images were reconstructed into apparent spatial resolutions of 0.7 × 0.8 × 1.5 mm. The acquisition time of each scan ranged from 3 to 4 minutes. The reduction in the echo-train spacing reduces the single-shot acquisition time, which effectively reduces motion-related artifacts and minimizes susceptibility effects, resulting in constant depiction of the peripheral vein throughout the cardiac cycle [6]. In addition, central k-space ordering reduces flow voids in the phase-encode direction. For these reasons, neither cardiac triggering nor a subtraction method was used.

Application of T-SLIPs

Two different oblique T-SLIPs were used (Fig. 1): One was placed on the liver and the thorax to cover the liver, heart, and thoracic descending aorta and suppress signal of the liver parenchyma, hepatic vein, and abdominal aorta. Its thickness was 150 mm. Four different TIs—800, 1,200, 1,600, and 2,000 milliseconds—were used to investigate the optimal TI for selective visualization of the portal venous system.

The other T-SLIP was placed on the lower abdomen caudad to the line between the inferior edge of the liver and the bifurcation of the abdominal aorta. The plane of this T-SLIP was oblique to minimize saturation of inflow signals to the liver from mesenteric veins and to suppress the ascending signal of the inferior vena cava (IVC) to the liver and avoid overlap of IVC signal with that of the portal vein. The thickness of this T-SLIP was 200 mm. The TI of this pulse was fixed to 1,100 milliseconds because it was near the null point of the venous blood [12] and gave enough time for the suppressed blood to flow into the upper abdominal region. The total scanning times were approximately 20 minutes, including scans at four different TIs for all volunteers.

Data Analysis

According to the difference in TIs of the T-SLIP placed on the liver and the thorax, four scanning parameter groups were created: group A, TIs of 800 and 1,100 milliseconds; group B, TIs of 1,200 and 1,100 milliseconds; group C, TIs of 1,600 and 1,100 milliseconds; and group D, TIs of 2,000 and 1,100 milliseconds. The acquired images were compared to detect the optimal TI for selective visualization of the portal venous system using maximum-intensity-projection (MIP) images and source images. All quantitative and qualitative assessments of image quality were performed on a commercially available workstation (Ziostation, Ziosoft).

Region-of-Interest (ROI) Analysis

On the coronal source images, ROIs were placed manually in the right portal vein (RPV) and left portal vein (LPV) and drawn as large as possible (mean, 48 mm^2; range, 26–77 mm^2). An ROI in the RPV was placed near the bifurcation of anterior and posterior segment branches, and an ROI in the LPV was placed in the umbilical portion. An ROI in the liver parenchyma was at least 40 mm^2 and was located in a homogeneous portion of the liver devoid of vessels and prominent artifacts and close to the portal vein. ROIs were drawn three times at each position, and the mean signal intensity (SI) values were adopted. Because the SD of the background noise could not be used to calculate the image signal-to-noise ratio (SNR) due to the use of the parallel imaging technique, we calculated SD of signal values in the ROI at the liver parenchyma as the noise (SD_{noise}) [13]. The SNR and contrast-to-noise ratio (CNR) were calculated using the following formulas:

$$SNR_{vessel} = SI_{vessel} / SD_{noise}$$

and

$$CNR_{vessel\text{-}liver} = (SI_{vessel} - SI_{liver}) / SD_{noise}.$$

SI_{liver} and SI_{vessel} are the mean signal intensity of ROIs in liver parenchyma and vessels—that is, the RPV and LPV, respectively. $CNR_{vessel\text{-}liver}$ is contrast-to-noise ratio of the vessels compared with the liver parenchyma.

Qualitative Analysis

The images were scored in consensus by two experienced radiologists (18 and 8 years of experience) who were blinded to the scanning conditions for visualization of the main trunk of the RPV and LPV and the portal branches of segments IV and VIII (P4 and P8, respectively). The visualization scores were evaluated using a 4-point scale: 1, not visible or nondiagnostic image quality; 2, poor image quality without sufficient visualization; 3, good image quality sufficient for diagnosis; or 4, excellent image quality with sharply defined vessels. Additional evaluation was conducted as to the overall image quality on arterial or venous overlap and motion artifact with a 3-point scale: 1, severe; 2, moderate; or 3, minimal [6].

Statistical Analysis

Statistical analyses were performed using a commercially available software package (Statview, version 5.0.1, SAS Institute). Comparisons of SNR and CNR were conducted using one-way repeated-measures analysis of variance followed by a post-hoc test. For the qualitative results of the different protocol groups, visualization scores and scores for overall image quality were compared using Friedman's nonparametric test and Scheffe's test.

A p value of less than 0.05 was taken to indicate a significant difference.

Results

Image acquisition was successfully conducted in all volunteers. The time required for image analysis was approximately 40 minutes per subject. The means and SDs of the SNRs and CNRs are shown in Table 1. Both were highest in group B. Signals of the liver parenchyma, hepatic arteries, and hepatic veins were adequately suppressed. In addition, high inflowing signals into the intrahepatic portal vein were obtained and peripheral portal venous branches were well visualized (Fig. 1). Statistically significant differences were also seen in SNR_{RPV}, $CNR_{RPV\text{-}liver}$, and $CNR_{LPV\text{-}liver}$ (contrast-to-noise ratio of the RPV and LPV compared with the liver parenchyma, respectively) between different groups (Table 1).

The results of qualitative analyses are shown in Table 2. Both the mean visualization scores of vessels and overall image quality were best in group B due to good visualization of the peripheral portal veins and sufficient signal suppression of the liver parenchyma and other vessels. There were significant differences between groups A and D ($p < 0.05$) and groups B and D ($p < 0.01$) in the visualization scores of the RPV. The visualization scores of the peripheral portal branches, such as P4 and P8, were better for groups B and C than the other groups; however, there was no statistically significant difference. Overall image quality was mainly influenced by overlapping signals of other vessels. Overall image quality was significantly worse for group D than for the other groups ($p < 0.01$) because of overlapping of other vessels, especially the

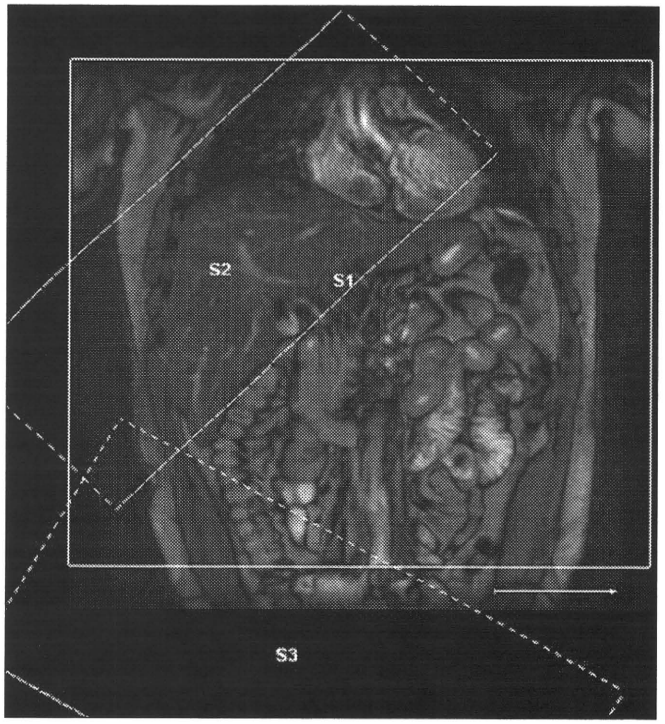

A

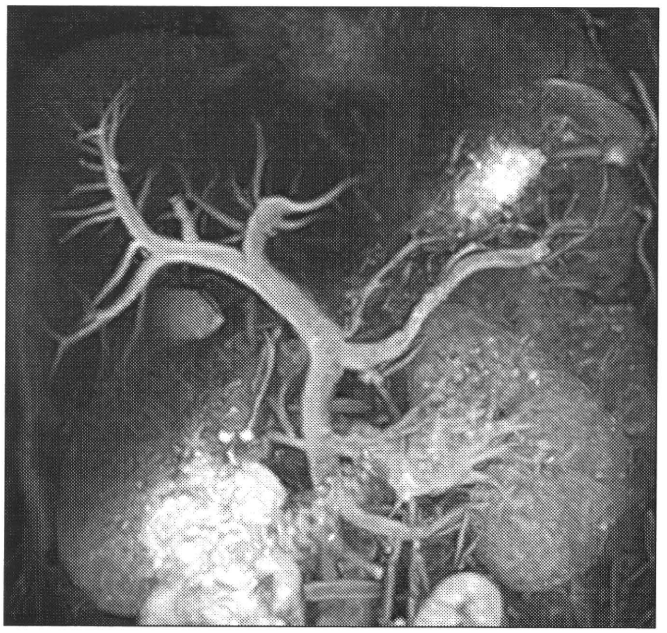

B

C

Fig. 1—Placement of two different oblique time–space labeling inversion pulses (T-SLIPs) for selective visualization of intrahepatic portal venous system.
A, On scout image of healthy 43-year-old male volunteer, one T-SLIP was placed on liver and thorax (S2) and other T-SLIP, on lower abdomen (S3). Rectangular area shows imaging volume (S1).
B and **C,** Coronal maximum-intensity-projection image (**B**) and source image (**C**) of 43-year-old male volunteer in group B (TIs of 1,200 and 1,100 milliseconds) show that portal venous system is selectively visualized in detail without exogenous contrast agent.

TABLE 1: Signal-to-Noise Ratio (SNR) and Contrast-to-Noise Ratio (CNR) Values in Each Group

Value	Group A	Group B	Group C	Group D
SNR_{RPV}	51.5 ± 18.6[a]	55.3 ± 24.5[b]	41.6 ± 19.4	34.8 ± 17.8
SNR_{LPV}	34.7 ± 10.6	43.6 ± 20.2	35.6 ± 15.4	31.6 ± 16.2
$CNR_{RPV\text{-}liver}$	41.2 ± 15.3[b]	44.7 ± 19.4[b,c]	32.1 ± 14.4	25.9 ± 13.1
$CNR_{LPV\text{-}liver}$	24.3 ± 9.8	32.9 ± 16.0[a]	26.1 ± 10.7	22.7 ± 11.5

Note—Data are means ± SD. RPV = right portal vein, LPV = left portal vein. $CNR_{RPV\text{-}liver}$ and $CNR_{LPV\text{-}liver}$ = contrast-to-noise ratio of the RPV and LPV compared with the liver parenchyma, respectively.
[a]Significantly better than group D ($p < 0.05$).
[b]Significantly better than group D ($p < 0.01$).
[c]Significantly better than group C ($p < 0.05$).

TABLE 2: Mean Visualization Scores and Overall Image Quality of Vessels in Each Group

Vessel	Group A	Group B	Group C	Group D
RPV	3.9 ± 0.3[a]	4.0[b]	3.8 ± 0.1	3.6 ± 0.6
LPV	3.6 ± 0.7	3.9 ± 0.2	3.8 ± 0.4	3.6 ± 0.6
P4	3.0 ± 1.0	3.7 ± 0.7	3.7 ± 0.6	3.1 ± 0.8
P8	3.5 ± 0.9	3.9 ± 0.3	3.8 ± 0.4	3.5 ± 0.7
Overall image quality	2.7 ± 0.4[b]	2.9 ± 0.3[b,c]	2.6 ± 0.5[b]	2.0 ± 0.5

Note—Data are means ± SD. Visualization of the LPV, P4, and P8 of groups B and C was better than groups A and D without significant statistical difference. RPV = right portal vein, LPV = left portal vein, P4 = peripheral branch in segment IV, P8 = peripheral branch in segment VIII.
[a]Significantly better than group D ($p < 0.05$).
[b]Significantly better than group D ($p < 0.01$).
[c]Significantly better than group C ($p < 0.05$).

hepatic vein; in addition, image quality of group B was significantly better than that of group C ($p < 0.05$).

The differences in image quality among the groups are presented in Figure 2. In group A, the TI of 800 milliseconds was not enough for inflowing portal flow to reach the periphery. On the other hand, the TI of 2,000 milliseconds in group D allowed signal recovery of the liver parenchyma and hepatic veins, and the peripheral portal venous signal sometimes became unclear in MIP images. Intrahepatic portal venous anatomy was well visualized in all subjects (Fig. 3). There were three cases of right anterior branch arising from the LPV.

Discussion

A detailed map of the portal venous anatomy is an important tool for surgeons to plan hepatic resection and living related donor liver transplantation [14–16]. In the past, conventional angiography was the standard method for visualization of the portal venous anatomy. More recently, MDCT has been playing one of the most important roles in the assessment of liver anatomy owing to its easy accessibility and its shorter examination time. This might reduce the need for multitechnique evaluation protocols [17]. However, the necessity of administering considerable volumes of potentially nephrotoxic iodinated contrast agents and of exposure to ionizing radiation are considerable disadvantages of the CT protocol.

On the other hand, MRA has been established as a valuable technique in detecting vascular disease without radiation exposure. In previous studies, 3D contrast-enhanced MR portography has been shown to be as effective as digital subtraction angiography for assessing the portal vein [18, 19]. Although MR contrast agents were thought to be much safer than CT contrast media, a serious adverse reaction called nephrogenic systemic fibrosis has recently been reported to occur after exposure to gadolinium-based contrast agents [20]. Hence, selective visualization of the portal vein with unenhanced MRA would be beneficial for the patient.

Half-Fourier FSE is one of the new unenhanced MRA techniques [21]. It allows coronal acquisition, which is not possible with time-of-flight imaging, especially for body MRA, and thus enables shorter 3D acquisition time [22, 23]. In addition, this sequence is T2-weighted and the liver parenchyma becomes relatively low signal intensity, resulting in good contrast between the portal vein and liver parenchyma; however, the long TE decreases the signal at the portal confluence where higher flow velocity might cause flow void in comparison with images acquired with true SSFP [1]. Also, selective visualization of the portal vein by this technique alone is not feasible.

Application of T-SLIPs in this study resulted in good signal suppression of the liver parenchyma and the vessels of no interest, which allowed selective visualization of the intrahepatic portal venous system without the use of contrast medium. When quantitative and qualitative analyses are summarized, the images of group B (TIs = 1,200 and 1,100 milliseconds) were the best and were optimal because the T-SLIP with those TIs attained both signal suppression of the liver parenchyma and vessels of no interest and inflow of portal venous signal to the periphery. The mean portal venous peak velocity has been reported to be 19.5 cm/s [24], so a TI of 1,200 milliseconds was considered sufficient for peripheral portal venous visualization. In group A, the TI of 800 milliseconds was not enough for inflowing portal flow to reach the periphery, so the visualization score of the peripheral branches (P4 and P8) was lower than in group B. On the other hand, the TI of 2,000 milliseconds in group D induced signal recovery of the liver parenchyma and hepatic veins and led to deterioration of the CNR.

Other structures that overlapped with the portal vein were the IVC and the biliary tract. Complete suppression of the IVC was not attained in all subjects because the T-SLIP on the lower abdomen did not cover the entire area of the IVC. The T-SLIP was placed to suppress the IVC signal, but at the same time, it was required to minimize suppression of blood signals in the superior and inferior mesenteric veins that flow into the portal vein. The ambivalence had resulted in incomplete suppression of the IVC in some subjects. Also biliary tracts sometimes overlapped with the portal vein in MIP images; however, by using source images in combination with MIP images, it did not cause a substantial problem to evaluate the intrahepatic portal vein.

Compared with contrast-enhanced MRA, our technique has several advantages. In general, high contrast between the portal vein and surrounding tissue is difficult to attain using contrast material because signals of

the liver parenchyma have already been high in the portal venous phase [2, 25]. In addition, to obtain high-level contrast between the vessels and surrounding tissue using contrast-enhanced MRA, data acquisition must be performed within a brief acquisition window during the first pass of the contrast agent [26]. Hence, optimal bolus timing is crucial and all data must be acquired during a single breath-hold, which limits spatial resolution [27]. On the contrary, there is no time constraint in our approach and it facilitates data acquisition for increased spatial resolution even in patients with a reduced breath-hold capability due to the use of respiratory-gating technology. Additionally, our approach dispels concerns about the adverse effects of contrast agents such as anaphylactic shock.

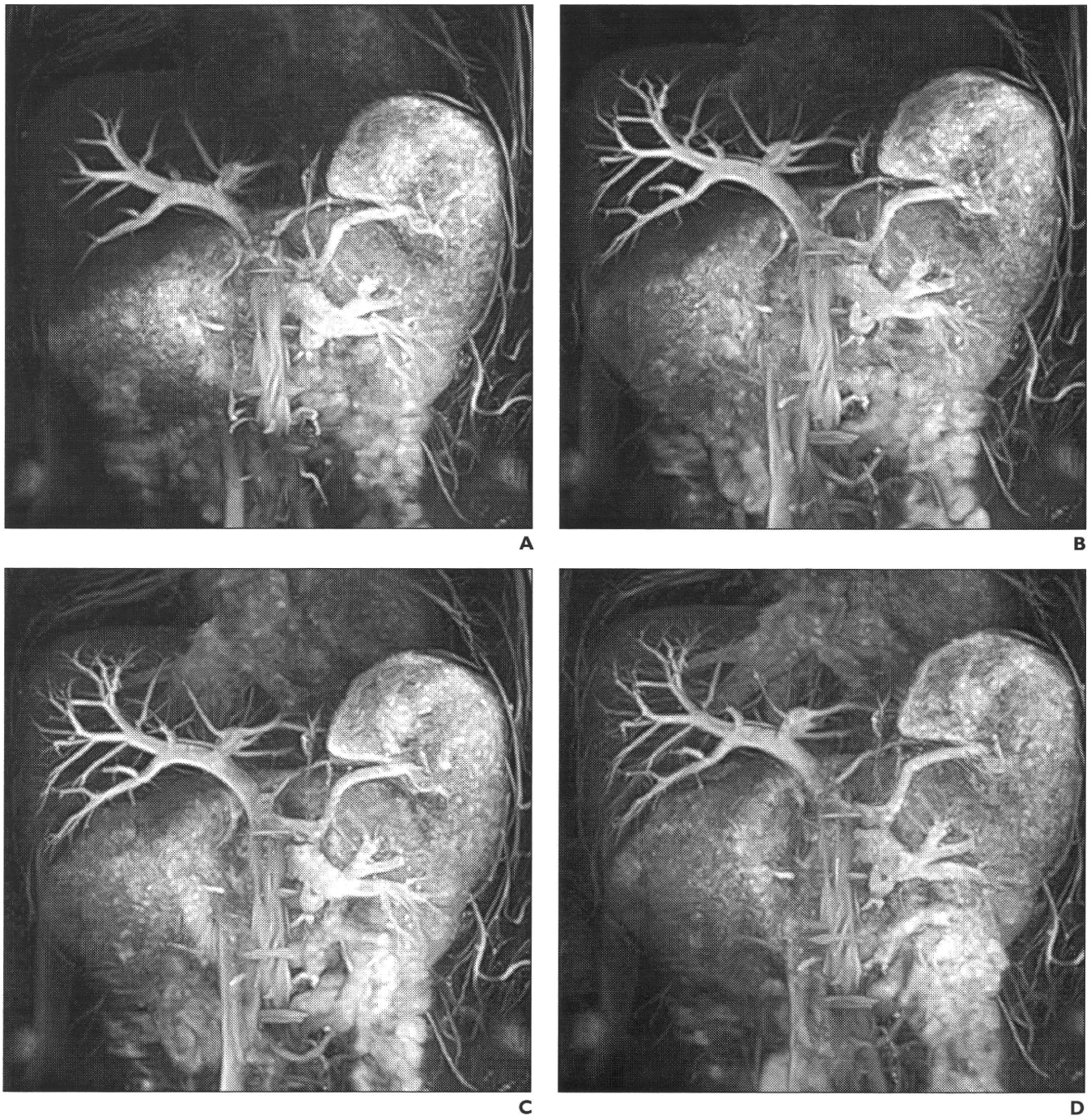

Fig. 2—Image quality differs depending on inversion time (TI).
A–D, Coronal maximum-intensity-projection images of healthy 40-year-old male volunteer illustrate changes between groups with different TIs: group A (**A**), 800 and 1,100 milliseconds; group B (**B**), 1,200 and 1,100 milliseconds; group C (**C**), 1,600 and 1,100 milliseconds; and group D (**D**), 2,000 and 1,100 milliseconds. Gradual portal venous inflow into periphery and signal recovery of liver parenchyma and hepatic veins were observed concurrently when TI was increased.

A

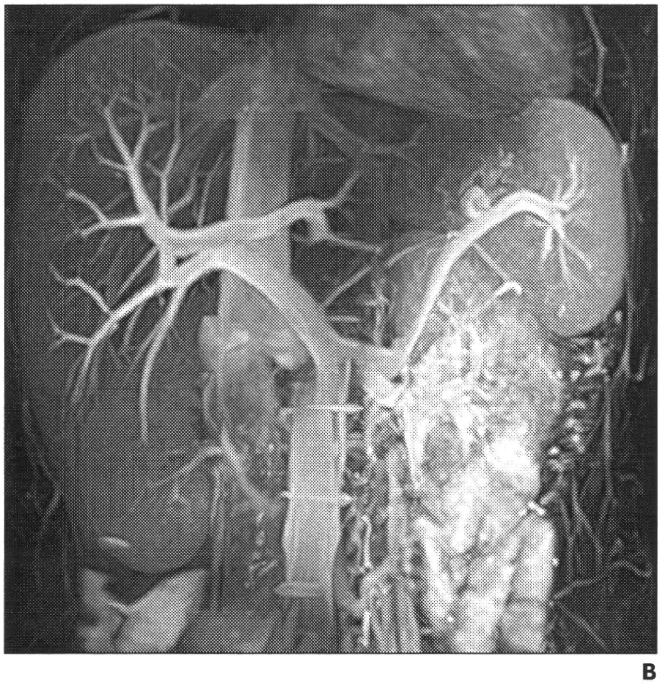

B

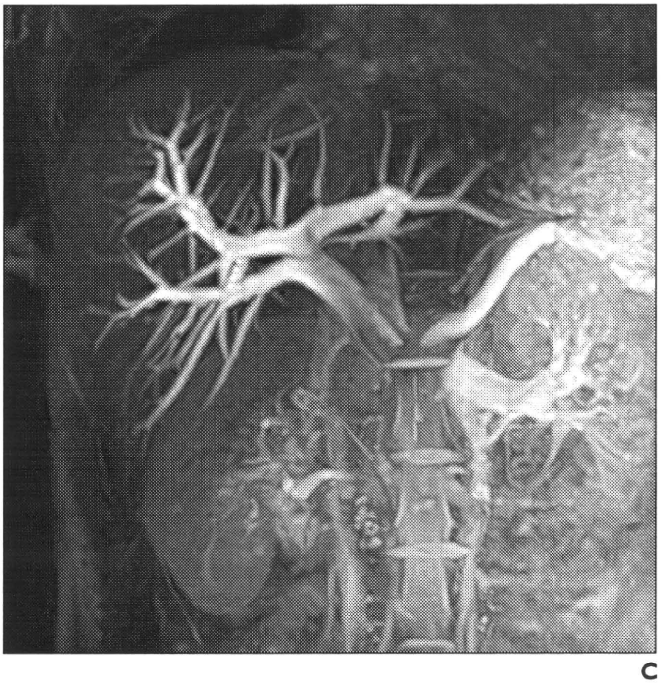

C

Fig. 3—Normal anatomy and anatomic variations of portal vein were visualized. **A,** Coronal maximum-intensity-projection (MIP) image of healthy 28-year-old male volunteer in group B (TIs, 1,200 and 1,100 milliseconds) shows normal portal bifurcation. Peripheral portal venous branches are also well seen.
B and **C,** Coronal MIP images of healthy 23-year-old female volunteer in group C (**B**) (TIs, 1,600 and 1,100 milliseconds) and healthy 27-year-old male volunteer in group B (**C**) (TIs, 1,200 and 1,100 milliseconds). Both images show normal variation of portal vein that right posterior branch diverges directly from main trunk and right anterior branch arises from left portal vein.

Patients with severe renal impairment can undergo this examination.

Our study had several limitations. The main limitation was the absence of a reference standard with which to compare the results of our qualitative analysis. Hepatic angiography or surgical exploration would have provided a more definitive determination of the portal venous anatomy in each subject, but this study aimed at optimization of the scanning parameters, and a comparative study with a reference standard is our next aim. Another limitation is that only healthy adult subjects were examined. The proposed method is dependent on inflow of portal signal, but it is reduced or even reversed in some patients with portal hypertension [28]. In addition, visualization of the distal portal branches might be impaired, and longer TIs, such as 1,600 milliseconds, would be better than 1,200 milliseconds despite the decrease in CNR by signal recovery of the liver parenchyma. Further studies will involve a larger sample size and include patients with conditions requiring visualization of the portal venous anatomy.

In conclusion, the combination of a respiratory-triggered 3D half-Fourier FSE sequence and T-SLIPs enabled selective visualization of the intrahepatic portal vein during

free breathing without an exogenous contrast agent. High contrast visualization was obtained while signals from other vessels and the liver parenchyma were adequately suppressed. Our preliminary data suggest that this technical approach has clinical promise.

Acknowledgments

We thank Nobuyasu Ichinose, Ayako Ninomiya, and Saori Satou (Toshiba Medical Systems Corporation) for their excellent technical assistance and advice on sequence optimization.

References

1. Smith CS, Sheehy N, McEniff N, Keogan MT. Magnetic resonance portal venography: use of fast-acquisition true FISP imaging in the detection of portal vein thrombosis. *Clin Radiol* 2007; 62:1180–1188
2. Lee MW, Lee JM, Lee JY, et al. Preoperative evaluation of hepatic arterial and portal venous anatomy using the time resolved echo-shared MR angiographic technique in living liver donors. *Eur Radiol* 2007; 17:1074–1080
3. Heilmaier C, Sutter R, Lutz AM, et al. Mapping of hepatic vascular anatomy: dynamic contrast-enhanced parallel MR imaging compared with 64 detector row CT. *Radiology* 2007; 245:872–880
4. Buhaescu I, Izzedine H. Gadolinium-induced nephrotoxicity. *Int J Clin Pract* 2008; 62:1113–1118
5. Katoh M, Spuentrup E, Stuber M, et al. Free-breathing renal magnetic resonance angiography with steady-state free-precession and slab-selective spin inversion combined with radial k-space sampling and water-selective excitation. *Magn Reson Med* 2005; 53:1228–1233
6. Miyazaki M, Takai H, Sugiura S, et al. Peripheral MR angiography: separation of arteries from veins with flow-spoiled gradient pulses in electrocardiography-triggered three-dimensional half-Fourier fast spin-echo imaging. *Radiology* 2003; 227:890–896
7. Weber OM, Martin AJ, Higgins CB. Whole-heart steady-state free precession coronary artery magnetic resonance angiography. *Magn Reson Med* 2003; 50:1223–1228
8. Shimada K, Isoda H, Okada T, et al. Non-contrast-enhanced hepatic MR angiography with true steady-state free-precession and time spatial labeling inversion pulse: optimization of the technique and preliminary results. *Eur J Radiol* 2008 Feb 2 [Epub ahead of print]
9. Ito K, Koike S, Jo C, et al. Intraportal venous flow distribution: evaluation with single breath-hold ECG-triggered three-dimensional half-Fourier fast spin-echo MR imaging and a selective inversion-recovery tagging pulse. *AJR* 2002; 178: 343–348
10. Constable RT, Gore JC. The loss of small objects in variable TE imaging: implications for FSE, RARE, and EPI. *Magn Reson Med* 1992; 28:9–24
11. Garcia DM, Duhamel G, Alsop DC. Efficiency of inversion pulses for background suppressed arterial spin labeling. *Magn Reson Med* 2005; 54: 366–372
12. Bernstein MA, King FK, Zhou XJ. *Handbook of MRI pulse sequences*. London, UK: Elsevier Academic Press, 2004:960–962
13. Isoda H, Kataoka M, Maetani Y, et al. MRCP imaging at 3.0 T vs. 1.5 T: preliminary experience in healthy volunteers. *J Magn Reson Imaging* 2007; 25:1000–1006
14. Curley SA, Chase JL, Roh MS, Hohn DC. Technical considerations and complications associated with the placement of 180 implantable arterial infusion devices. *Surgery* 1993; 114:928–935
15. Guiney MJ, Kruskal JB, Sosna J, et al. Multi-detector row CT vascular anatomy of the surgical plane in split-liver transplantation. *Radiology* 2003; 229:401–407
16. Kapoor V, Brancatelli G, Federle MP, Katyal S, Marsh JW, Geller DA. Multidetector CT arteriography with volumetric three-dimensional rendering to evaluate patients with metastatic colorectal disease for placement of a floxuridine infusion pump. *AJR* 2003; 181:455–463
17. Schroeder T, Malago M, Debatin JF, et al. "All-in-one" imaging protocols for the evaluation of potential living liver donors: comparison of magnetic resonance imaging and multidetector computed tomography. *Liver Transpl* 2005; 11:776–787
18. Kreft B, Strunk H, Flacke S, et al. Detection of thrombosis in the portal venous system: comparison of contrast-enhanced MR angiography with intraarterial digital subtraction angiography. *Radiology* 2000; 216:86–92
19. Ito K, Blasbalg R, Hussain SM, Mitchell DG. Portal vein and its tributaries: evaluation with thin-section three-dimensional contrast-enhanced dynamic fat-suppressed MR imaging. *Radiology* 2000; 215:381–386
20. Marckmann P, Skov L, Rossen K, et al. Nephrogenic systemic fibrosis: suspected etiological role of gadodiamide used for contrast-enhanced magnetic resonance imaging. *J Am Soc Nephrol* 2006; 17:2359–2362
21. Miyazaki M, Lee VS. Nonenhanced MR angiography. *Radiology* 2008; 248:20–43
22. Miyazaki M, Sugiura S, Tateishi F, Wada H, Kassai Y, Abe H. Non-contrast-enhanced MR angiography using 3D ECG-synchronized half-Fourier fast spin echo. *J Magn Reson Imaging* 2000; 12:776–783
23. Miyazaki M, Ichinose N, Sugiura S, et al. A novel MR angiography technique: swap phase encode extended data (SPEED) acquisition using half-Fourier RARE. *J Magn Reson Imaging* 1998; 8:505–507
24. Sugimoto H, Kaneko T, Hirota M, Inoue S, Takeda S, Nakao A. Physical hemodynamic interaction between portal venous and hepatic arterial blood flow in humans. *Liver Int* 2005; 25: 282–287
25. Lim JS, Kim MJ, Kim JH, et al. Preoperative MRI of potential living-donor-related liver transplantation using a single dose of gadobenate dimeglumine. *AJR* 2005; 185:424–431
26. Grist TM. Magnetic resonance angiography of renal arterial stenosis. *Coron Artery Dis* 1999; 10:151–156
27. Maki JH, Chenevert TL, Prince MR. Contrast-enhanced MR angiography. *Abdom Imaging* 1998; 23:469–484
28. Gaiani S, Bolondi L, Li Bassi S, Zironi G, Siringo S, Barbara L. Prevalence of spontaneous hepatofugal portal flow in liver cirrhosis: clinical and endoscopic correlation in 228 patients. *Gastroenterology* 1991; 100:160–167